Hodographs and Skew *T*s of Hail-Producing Storms

CAMERON J. NIXON,[a] JOHN T. ALLEN,[a] AND MATEUSZ TASZAREK[b]

[a] *Department of Earth and Atmospheric Sciences, Central Michigan University, Mt. Pleasant, Michigan*
[b] *Department of Meteorology and Climatology, Adam Mickiewicz University, Poznan, Poland*

(Manuscript received 23 February 2023, in final form 29 August 2023, accepted 1 September 2023)

ABSTRACT: Environments associated with severe hailstorms, compared to those of tornadoes, are often less apparent to forecasters. Understanding has evolved considerably in recent years; namely, that weak low-level shear and sufficient convective available potential energy (CAPE) above the freezing level is most favorable for large hail. However, this understanding comes only from examining the mean characteristics of large hail environments. How much variety exists within the kinematic and thermodynamic environments of large hail? Is there a balance between shear and CAPE analogous to that noted with tornadoes? We address these questions to move toward a more complete conceptual model. In this study, we investigate the environments of 92 323 hail reports (both severe and nonsevere) using ERA5 modeled proximity soundings. By employing a self-organizing map algorithm and subsetting these environments by a multitude of characteristics, we find that the conditions leading to large hail are highly variable, but three primary patterns emerge. First, hail growth depends on a favorable balance of CAPE, wind shear, and relative humidity, such that accounting for entrainment is important in parameter-based hail prediction. Second, hail growth is thwarted by strong low-level storm-relative winds, unless CAPE below the hail growth zone is weak. Finally, the maximum hail size possible in a given environment may be predictable by the depth of buoyancy, rather than CAPE itself.

KEYWORDS: Hail; Forecasting; Forecasting techniques; Mesoscale forecasting; Nowcasting; Operational forecasting

1. Introduction

Background

Of severe thunderstorm hazards, severe hail is the most expensive in the United States, incurring around $10 billion (USD) in insured losses annually, and up to $1 billion in a single event (Gunturi and Tippett 2017). Significant-severe hail (≥2.0 in.) has particularly damaging safety/economic impacts (Hales 1988; Johnson and Sugden 2014; Blair et al. 2017). Compared to tornadoes, literature on hail and its dependency on the near-storm environment is less abundant.

Traditionally, the thermodynamic profile has been treated as critical in hail forecasting. Indeed, hail growth depends on a favorable temperature range (Nelson 1983; Browning and Foote 1976; Miller et al. 1988; Knight and Knight 2001), such that an updraft that fails to extend into subfreezing air aloft will simply not produce hail. The layer between −10° and −30°C is generally considered as optimal for hail growth (Nelson 1983; Browning and Foote 1976; Miller et al. 1988; Knight and Knight 2001; Pilorz et al. 2022), and is often appropriately termed the "hail growth zone" (HGZ). This layer varies in height for any given storm, but is generally in the midlevels of the troposphere. Both cloud models (Brimelow et al. 2002; Kumjian and Lombardo 2020) and observational studies (Knight and Knight 2005) have shown that hail grows almost exclusively in subfreezing temperatures. As hailstones fall into warmer temperatures, they can melt before reaching the ground, but this disproportionately reduces the mass of smaller stones due to their slower fall speeds and larger surface-area-to-mass ratio (Rasmussen and Heymsfield 1987).

Proxies for updraft buoyancy [such as convective available potential energy (CAPE) and temperature lapse rates] have also shown some skill in hail size forecasting (Groenemeijer and Van Delden 2007; Johnson and Sugden 2014; Púčik et al. 2015; Taszarek et al. 2017, 2020). However, owing to the limitations of parcel theory, CAPE can be an unrealistic approximation. An updraft's net total buoyancy depends not only on CAPE, but also on how much CAPE is lost through the entrainment of air outside the updraft. While wider updrafts are more resistant to entrainment, narrower updrafts are more readily diluted, especially in drier tropospheres (Holton 1973; Kuo and Raymond 1980; Peters et al. 2019, 2023). Updraft width depends strongly on mixed-layer depth (Mulholland et al. 2021) and the mass flux provided by storm-relative inflow (Peters et al. 2020a,b; Lasher-Trapp et al. 2021). Consequently, CAPE can be maximized with higher relative humidity, deeper mixed layers, and stronger storm-relative inflow. Indeed, stronger deep-layer shear that induces stronger storm-relative inflow has been found in simulations to support broader updrafts that produce more hail embryos and increase their residence time aloft (Dennis and Kumjian 2017; Kumjian et al. 2021). A "balance" between CAPE and shear has been noted throughout literature, such that more favorable kinematics can supplement less favorable thermodynamics, and vice versa (Johns et al. 1993; Brooks et al. 2003; Brooks 2009; Taszarek et al. 2020).

Observational and modeling studies have also linked hail potential to the shear profile. Storm-relative winds have been considered critical in regulating hail growth since the 1970s. An observational study by Browning and Foote (1976) was among

Denotes content that is immediately available upon publication as open access.

Corresponding author: Cameron J. Nixon, cameron.nixon@cmich.edu

DOI: 10.1175/WAF-D-23-0031.1

the first to recognize that the ice nuclei responsible for hail formation are supplied by the flanking line of a supercell—a series of weak but progressively maturing updrafts. Since this region consisted of hail "embryos," it was termed the "embryo curtain." This flanking line was thought to be induced by a stagnation point between two diverting midlevel flow streams. Nelson (1983) deduced that updraft-relative flow within this flanking line fundamentally modulated the residence time of embryos within it, and thus their propensity to grow. In theory, this residence time would be maximized by moderately strong updrafts (i.e., strong enough but not intense), and slow storm-relative flow (Rasmussen and Heymsfield 1987).

How exactly storm-relative wind governs hail trajectories is a topic of current investigation. Stronger low-level shear, especially that is directed obliquely to the deep-layer shear (such that creates a sickle-shaped hodograph) has been found to suppress hail growth (Dennis and Kumjian 2017; Kumjian et al. 2021). This suppression is attributed to an increase in low-level storm-relative winds, which can impart excessive momentum on air parcels as they approach the hail growth zone. Consequently, excessive updraft-relative flow within the hail growth zone can limit the residence time of any hailstones within it (Kumjian et al. 2021; Lin and Kumjian 2022). Literature has not yet clarified whether this process is predictable solely by the storm-relative winds or also in part to the shear or its direction. Regardless, recent observational studies unambiguously find large hail environments to be associated with relatively weak shear in the lowest 1 km (Johnson and Sugden 2014; Kumjian et al. 2019; Gutierrez and Kumjian 2021; Taszarek et al. 2020; Nixon and Allen 2022). Idealized simulations have found that unfavorable trajectories may also be induced by excess CAPE, and may similarly limit a hailstone's residence time in optimal conditions (Lin and Kumjian 2022).

This study investigates three critical yet contradictory relationships between hail and the near-storm environment. First, although stronger CAPE and deep-layer shear can support stronger updrafts, these profiles alone, when taken in the mean sense, have shown surprisingly weak skill in predicting hail size (Johnson and Sugden 2014; Gensini et al. 2021; Nixon and Allen 2022). Recent literature even suggests that both CAPE and shear behave nonlinearly, such that increasing buoyancy (Lin and Kumjian 2022) and shear (Dennis and Kumjian 2017) in certain layers can have detrimental impacts on hail trajectories and growth potential beyond an "optimal" amount. So while increasing CAPE and shear may be more favorable for hail occurrence (Taszarek et al. 2020), this may not always be true for hail size, as is assumed in some parameters (e.g., Johnson and Sugden 2014).

Second, although stronger storm-relative inflow may support larger updrafts that can supply more hail embryos (Dennis and Kumjian 2017; Kumjian et al. 2021), it may also shorten the residence time of hailstones in the hail growth zone (Dennis and Kumjian 2017; Kumjian et al. 2021; Lin and Kumjian 2022). It is not known whether these impacts are primarily a result of the storm-relative winds, or also the low-level wind shear itself—this is an important, unresolved problem for forecast applications.

Last, although temperature is fundamental in hail growth, attempts to incorporate this dimension into the forecast process have so far been met with confusion. Counterintuitively, neither freezing level height nor CAPE within the hail growth zone add significant value to hail size forecasting, and the thickness of the hail growth zone itself has actually been shown to *decrease* with increasing hail size, at least in the United States (Johnson and Sugden 2014). It is not clear why temperature, a critical control of hail growth, has shown little practical utility so far in forecasting.

These contradictions motivate three main hypotheses:

1) A balance of CAPE, shear, and relative humidity (such that all affect net CAPE after entrainment) is necessary for hail growth.
2) Strong low-level storm-relative wind is unfavorable for hail growth, except in certain thermodynamic environments
3) The depth of CAPE (not CAPE itself), particularly above the freezing level, inextricably controls hail growth and potential size.

These hypotheses challenge the efficacy of our most commonly used parameters for hail prediction. Though stronger deep-layer bulk wind difference is thought to support stronger supercells more capable of hail production, there is already evidence that shear can be more or *less* favorable depending on its height in the profile. Though larger CAPE and steeper midlevel lapse rates are thought to support stronger updrafts capable of lofting larger hail, this assumes that these parameters are good estimates of updraft speeds, and that larger hail actually needs stronger updrafts in the first place. In light of recent literature, we question these assumptions. Rather, we believe that parameterizations of updraft width, updraft depth, storm-relative flow, and the freezing level are just as critical to large hail prediction.

2. Data and methods

a. Case selection

This study uses a new dataset developed by Allen et al. (2023, manuscript submitted to *Wea. Forecasting*), which amasses independent hail reports from multiple sources of sizes ranging from 2.5 to 200 mm. Hail events in excess of 100 mm were cross validated using radar data for plausibility. The dataset includes portions derived from the hazard–storm mode dataset developed by the Storm Prediction Center (Smith et al. 2012; Thompson et al. 2012), for the period 2005–17 (most reports coming from 2014 to 2015), the *Storm Data* database (Schaefer and Edwards 1999) from 1990 to 2019, the Community Collaborative Rain, Hail and Snow network (CoCoRaHS; Reges et al. 2016) for the period 1998–2019 and mPING (Elmore et al. 2014, 2022) for the period 2012–19. The net result is a dataset which, unlike any prior study, includes nearly a quarter of its reports smaller than 1 in. (25 mm), since data below 19 mm are not found within *Storm Data* (Elmore et al. 2022).

Unlike prior bulk approaches with *Storm Data*, the dataset is designed to ensure independent and reliable cases. Reports on the same day are queried to maintain a minimum separation of 75 km in space, with duplicate reports in the same vicinity discarded in favor of the largest hail event observed in

that environment. Sampling an environment from a given grid point only once on a single day is used to avoid convective contamination issues that may arise with activation of the convective parameterization scheme (Allen and Karoly 2014). Unlike the hazard-storm mode dataset (Smith et al. 2012; Thompson et al. 2012), this dataset does not contain information on convective mode. All cases with less than 250 J kg^{-1} CAPE were omitted for this study prior to any analysis, in an effort to minimize cases that may have had inaccurate report times, or cases where model data did not accurately resolve the position of boundaries (e.g., Potvin et al. 2010). After this removal, this study considers 92 323 cases of hail. We will subsequently refer to hail smaller than 1 in. (25 mm) as "subsevere" (Kumjian et al. 2019), 1–1.75 in. (25–45 mm) as "severe," 2–3.75 in. (50–95 mm) as "sig.-severe," and greater than 4 in. (102 mm) as "giant" (Knight and Knight 2001). More generally, "large" is used throughout to refer to hail of at least 1 in.

The imperfect nature of reporting will always affect report-based observational datasets such as those used in this study, and hence we rely on a larger sample size to offset the uncertainty this may introduce in distinguishing between classes. Humans do not always accurately report hail times, locations, or sizes (Schaefer and Galway 1982; Amburn and Wolf 1997; Baumgardt 2011; Allen et al. 2015; Allen and Tippett 2015). This may affect the size bin that reports are put into (Jewell and Brimelow 2009; Schaefer et al. 2004), and as a result may increase the difficulty of using parameters to distinguish between sizes that are close to size thresholds. In addition, the probability and density of hail reports is biased toward population density, where more people are available to make them (Dobur 2005; Blair and Leighton 2012; Groenemeijer et al. 2017; Allen et al. 2020). This can impact environmental parameters by leading to oversampling where observations are more frequent, potentially biasing against events which occur in more remote areas. Reports are also more likely during the day when more people are awake, which may exclude representative samples of nocturnal cases (Ashley et al. 2008; Blair et al. 2017). The priority placed on seeking hail reports may vary per event, and per National Weather Service Weather Forecast Office (Doswell et al. 2005). Hail reporting may also be deferred during life-threatening events (such as a tornado), possibly causing it to go unreported during tornadoes (Warren et al. 2021), but this has not yet been investigated in published literature.

b. *Environmental data*

Environmental data for each case were obtained from the fifth-generation ECMWF reanalysis (ERA5; Copernicus Climate Change Service 2017; Hersbach et al. 2020). This reanalysis has been shown to faithfully represent the vertical profiles of severe convective events in the United States and Europe (Coffer et al. 2020; Taszarek et al. 2021b; Pilguj et al. 2022), but still, some known biases exist. Like many reanalysis and model analysis products, the profiles derived from these data show the largest biases in the boundary layer (Gensini et al. 2014; Taszarek et al. 2018; King and Kennedy 2019; Taszarek et al. 2021b). In particular, some of the largest differences between ERA5 reanalyses and observed soundings have been found in low-level convective parcel parameters and low-level shear, especially in proximity to surface boundaries (Taszarek et al. 2021b). These biases also differ per geographic location and surface elevation. Though this study is concerned with more deep-layer features such as bulk shear, CAPE and its depth, and relative humidity, we also examine the relationship between CAPE and shear in the low levels. As explored later, reports are from a variety of locations and elevations across the United States. Thus, conclusions drawn from this study, especially on the relationship between low-level CAPE and shear, are based on assumptions that ERA5 accurately represents the boundary layer profiles of these cases, and does so consistently regardless of location. Fortunately, however, ERA5 is still one of the most reliable reanalyses for convective environments (Coffer et al. 2020; Taszarek et al. 2021b).

TABLE 1. Environmental parameters.

	Definition
S01	Bulk wind difference (0–1 km)
S06	Bulk wind difference (0–6 km)
SRW01	Storm-relative wind (0–1-km mean)
RH13	Relative humidity (1–3-km mean)
RH16	Relative humidity (1–6-km mean)
LCL	Lifted condensation level (SB parcel)
EIB	Effective inflow base
LPL	Lifted parcel level (MU parcel)
LFC	Level of free convection (MU parcel)
MPL	Maximum parcel level (MU parcel)
CAPE	Convective available potential energy (MU parcel)
HGZ CAPE	CAPE between −10° and −30°C (MU parcel)
Sub-HGZ CAPE	CAPE below −10°C (MU parcel)
CIN	Convective inhibition (SB parcel)
FZL	Freezing level (MU parcel)
HGZ	Hail growth zone (layer from −10° to −30°C, MU parcel)

Vertical profiles were obtained from hybrid sigma-pressure level ERA5 data. To ensure comparable vertical resolutions upon compositing, profiles used in composites were interpolated to a common 250 m. This spacing was chosen to ensure a balance between computational cost and resolution of the environmental features relevant for hail. Profiles were taken at the closest grid point to the latitude and longitude of each report. This study does not employ a design such as is suggested in Potvin et al. (2010) to minimize the impacts of convective contamination using spatial offsetting, but it does aim for preconvective conditions by using the analysis hour rounded down to the top of the hour preceding each report (in accordance with Thompson et al. 2012). For instance, a report at 2045 UTC would be represented with a 2000 UTC ERA5 sounding.

All derived kinematic and thermodynamic variables used in this study were calculated from their respective raw hybrid sigma-pressure level ERA5 profiles using xcape (https://github.com/xgcm/xcape). A list of variable abbreviations and their meanings can be found in Table 1. The kinematic variables used include bulk wind difference in the 0–6-km (S06) and 0–1-km (S01) layers, and the mean storm-relative wind from 0 to 1 km

(SRW01), all with units of meters per second (m s^{-1}). Storm-relative wind was subject to assumptions on storm motion, since neither observed storm motions, supercell type (right-moving or left-moving) nor storm mode (supercell, multicell cluster, squall line, etc.) were recorded for this dataset. To account for this, storm motion was calculated by assuming a right-moving supercell storm motion (Bunkers et al. 2000) for all cases with S06 $\geq$ 15 m s^{-1} (similar to Houston et al. 2008). For cases with S06 $<$ 15 m s^{-1}, a supercell was not assumed, and storm motion was assumed to be the 0–6-km non-pressure-weighted mean wind (Bunkers et al. 2000). Although left-moving supercells were assumed to make up a portion of this dataset (as explored by Nixon and Allen 2022), no assumptions were made as to whether cases were associated with a left-moving supercell. Rather, a right-moving supercell was always assumed for S06 $\geq$ 15 m s^{-1}. Though this introduces inaccuracies into the storm-relative wind profiles of any left-moving supercell cases, the shear profiles in this sample were fortunately predominantly straight. As a result, SRW01 (the most closely examined storm-relative wind parameter herein) varied little between right-moving and left-moving supercells—less than 1.5 m s^{-1} per case on average.

The thermodynamic variables used in this study use either most-unstable (MU) and surface-based (SB) parcel profiles depending on their meteorological significance. CAPE (J kg^{-1}), level of free convection (LFC), and maximum parcel level (MPL) all assume the MU parcel, since this can be used in both surface-based and elevated storm scenarios (a significant portion of hailstorms was associated with elevated storms, as explored later). CIN (J kg^{-1}) and lifted condensation level (LCL) both assume the SB parcel, since this parcel best detects the degree of low-level stability, and the lowest potential cloud base, respectively, in both surface-based and elevated storm scenarios (e.g., in the case of a storm elevated above a stable layer, most-unstable CAPE is necessary to better approximate the maximum potential energy available to an updraft, but most-unstable CIN may considerably underestimate the CIN that this updraft experiences pulling parcels from the surface). The buoyancy profile is calculated using the virtual temperature correction. Where referenced, the most-unstable lifted parcel level (LPL) refers to the height of the most unstable parcel in the lowest 400 hPa (which may be different from the surface-based parcel especially in elevated storm scenarios). Other significant heights include the effective inflow base (EIB, Thompson et al. 2007) and the freezing level (FZL). All heights are measured in meters unless otherwise specified. The −10° and −30°C levels are used to calculate CAPE both within the HGZ (HGZ CAPE) and below the HGZ (sub-HGZ CAPE). This study also examines the relative humidity of the ambient air between 1–3 km (RH13) and 1–6 km (RH16), a proxy for lower-tropospheric RH above the cloud base where entrainment matters most (Peters et al. 2019), as a fraction from 0 to 1.0.

c. *Self-organizing maps*

A self-organizing map (SOM; Kohonen 2013) approach was used initially to find relevant environmental relationships and guide further investigations. A SOM can procure information on the variance of a sample, and can thus better detect the multiple different weather regimes found throughout the year and across the United States that are not apparent by examining the mean alone. The particular SOM application used can be found at https://github.com/JustGlowing/minisom. SOMs have been used to discriminate between the vertical profiles of tornadic and nontornadic storms (Nowotarski and Jensen 2013; Anderson-Frey et al. 2017; Nowotarski and Jones 2018). Warren et al. (2021) used SOMs to identify severe hail environments, while Zhou et al. (2021) used this technique to find that the environments of hailstorms vary across the globe. This study, unlike previous efforts, examines only cases of hail-producing storms using a very large sample of observed hailstorms, including both severe and subsevere reports, thus better representing the full distribution of hail sizes.

A SOM is a type of artificial neural network that sorts input data into an array of clusters ("nodes") in a two-dimensional space. Nodes are arranged in this space such that similar nodes are positioned closer together, and data can fall anywhere within the lattice of their positions. The number of nodes are user-specified, and can be chosen to optimize their distinctiveness from one another (Kohonen 2013). These nodes are initialized with random weights, and an input vector is initialized randomly from the input data. Then, the nearest node to the input vector is calculated (via Euclidean distance), along with the nearest neighbors. The process of selecting a new input vector and assigning data to clusters is repeated over multiple iterations to produce robust clusters. In this way, the SOM is an iterative and unsupervised learning process. For more information on SOMs and their application in meteorological tasks, the reader is directed to Chase et al. (2023) and the aforementioned studies that used them (e.g., Nowotarski and Jensen 2013; Anderson-Frey et al. 2017; Nowotarski and Jones 2018; Warren et al. 2021; Zhou et al. 2021).

In this study, SOMs were set up using a 3 × 3 matrix of nodes, following Nowotarski and Jensen (2013), Warren et al. (2021), and Anderson-Frey et al. (2017), who noted an optimal balance between the diversity and distinctiveness of the resulting nodes using this array size in large datasets of severe convective data. To ensure convergence, 200 iterations of this self-organizing map algorithm were used to train the nodes, since Anderson-Frey et al. (2017) noted that increasing more than 200 iterations held little extra benefit. Initially, SOMs were trained on hail cases of all sizes. However, since stones around 1 in. were disproportionately common in this dataset, the SOMs produced nodes with minimal environmental differences, and little difference in mean hail size. Since the goal of using SOMs was to find differences in the environment and its effect on hail size, this oversampling was undesirable. Instead, all cases of hail $\geq$ 12.5 mm and hail $<$ 50 mm were omitted from this sample; a total of 17 830 cases were then used in the SOMs.

Input to the SOMs are the interpolated vertical kinematic and thermodynamic profiles. The variables representing these profiles were selected to best preserve the most relevant features of each input profile. For the kinematic profile, hodograph shape (especially in the low levels) must be preserved

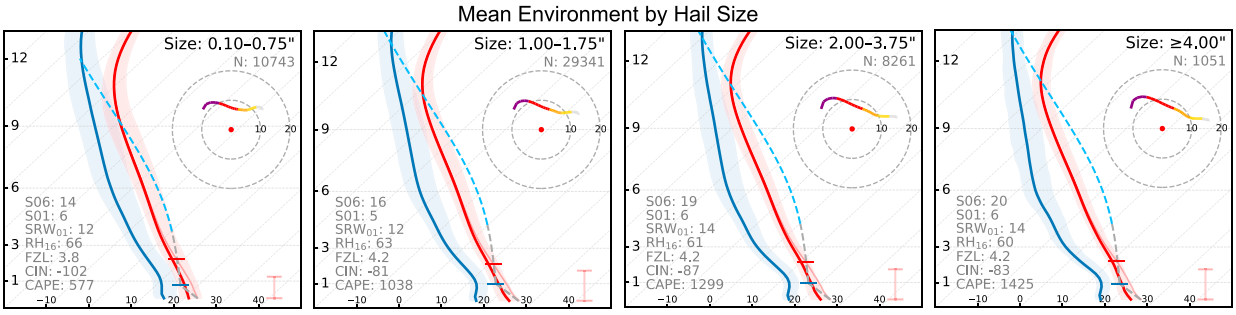

FIG. 1. Mean skew T and hodograph for subsevere hail, severe hail, significant-severe hail, and giant hail, shown from left to right, respectively. The mean skew T is composed of the dewpoint mean (blue line) and interquartile range (blue shading) for each sample, the temperature mean (red line) and interquartile range (red shading) for each sample, the most-unstable parcel path (dashed gray line, changing to blue above the FZL, truncated at the MPL) and surface-based parcel path (dashed gray line, if different from the most-unstable parcel path), the LCL (blue horizontal mark), the LFC (red horizontal mark), and the effective inflow layer (red line above the 40°C mark). The mean 0–3-km shear-relative hodograph is displayed in the storm-relative sense by subtracting the right-moving storm motion calculated from this mean profile, and is composed of the 0–1-km shear (purple), the 1–3-km shear (red), the 3–6-km shear (orange), the 6–9-km shear (gold), the 9–12-km shear (light yellow), and the storm motion (red dot at origin), with the 10 and 20 m s^{-1} storm-relative wind range rings plotted outside the storm motion (red). An assortment of parameters (their definitions and units defined in section 2) are plotted on left hand side of each panel; these are calculated using the mean profile. Height is in meters, temperature in degrees Celsius, and wind in meters per second.

in such a way that does not depend on storm motion, ground-relative speed, or direction. Before compositing, shear profiles were transformed by first rotating them by the direction of the 0–3-km shear vector (such that this vector lays parallel to the x axis), then subtracting the surface u and v wind (such that the hodograph starts at the origin). This methodology, which is used to better ensure that mean hodograph shapes represent their constituents, is described in more detail in Nixon and Allen (2022). These rotated shear-relative u and v components were inputs to the SOM. For the thermodynamic profile, temperature (T) must first be preserved, since hail growth depends on both buoyancy and favorable temperatures. Consequently, T was selected as an input. This differs from the solely buoyancy-preserving approach in Warren et al. (2021), which was necessary to cluster tornadic environments. Alongside T, the moisture profile must also be preserved. Though dewpoint was considered for this, it is a weak function of pressure, so it cannot consistently approximate water vapor mass or relative humidity across different elevations (Warren et al. 2021). Instead, mixing ratio (w), a more direct measure of water vapor content, was selected as an input.

Before the SOM was trained on these parameters, wind profiles were truncated to 9 km to minimize the influence of the upper-level wind profile (which was found to have considerable spread, especially in cases with low tropopauses), similar to Warren et al. (2021). We acknowledge that wind data above 9 km may still influence upper-level storm-relative flow, storm motion, and storm size (Warren et al. 2017). Thermodynamic profiles were considered up to 15 km in accordance with Warren et al. (2021), since some of the parameters examined herein (especially CAPE and MPL) depend on tropopause height and how high the buoyancy profile extends. Before these parameters were input to the SOM, they were normalized by subtracting the mean and dividing by the standard deviation of each parameter (at each height) across the entire input sample. According to Warren et al. (2021), this method better equalizes the weights of each parameter in the training of the SOM. Although it assumes that each parameter is normally distributed across the input sample, this assumption was deemed justifiable for both wind and temperature profiles by Warren et al. (2021). For all SOMs, the mean T, w, u, and v is obtained from each node, and used to reconstruct a representative hodograph and skew T.

Though this study identifies multiple relevant relationships using SOMs, it also employs strategic subsetting to further investigate them. Throughout this study, environments will be subset by percentile, such that "high" refers to all cases where a specified parameter is at least one standard deviation above the mean, and "low" refers to all cases where that parameter is less than one standard deviation below the mean (e.g., "high CAPE" will refer to any value of CAPE greater than or equal to the 84.1st percentile of CAPE, or one standard deviation above the mean of CAPE, assuming a normal distribution). This subsetting approach was used to display important environmental relationships in a more simple manner and to better highlight differences between environments.

3. Results

a. *Variance in the environments of hail-producing storms*

With the exception of Warren et al. (2021), most studies have examined hail environments statistically (e.g., Johnson and Sugden 2014; Taszarek et al. 2020; Gensini et al. 2021; Nixon and Allen 2022; Homeyer et al. 2023), focusing on mean environmental parameters and their spread. Because of the considerably larger size and improved robustness of the dataset used herein, we include the mean environments of hail binned by size in Fig. 1. Similar to Johnson and Sugden (2014), larger hail is

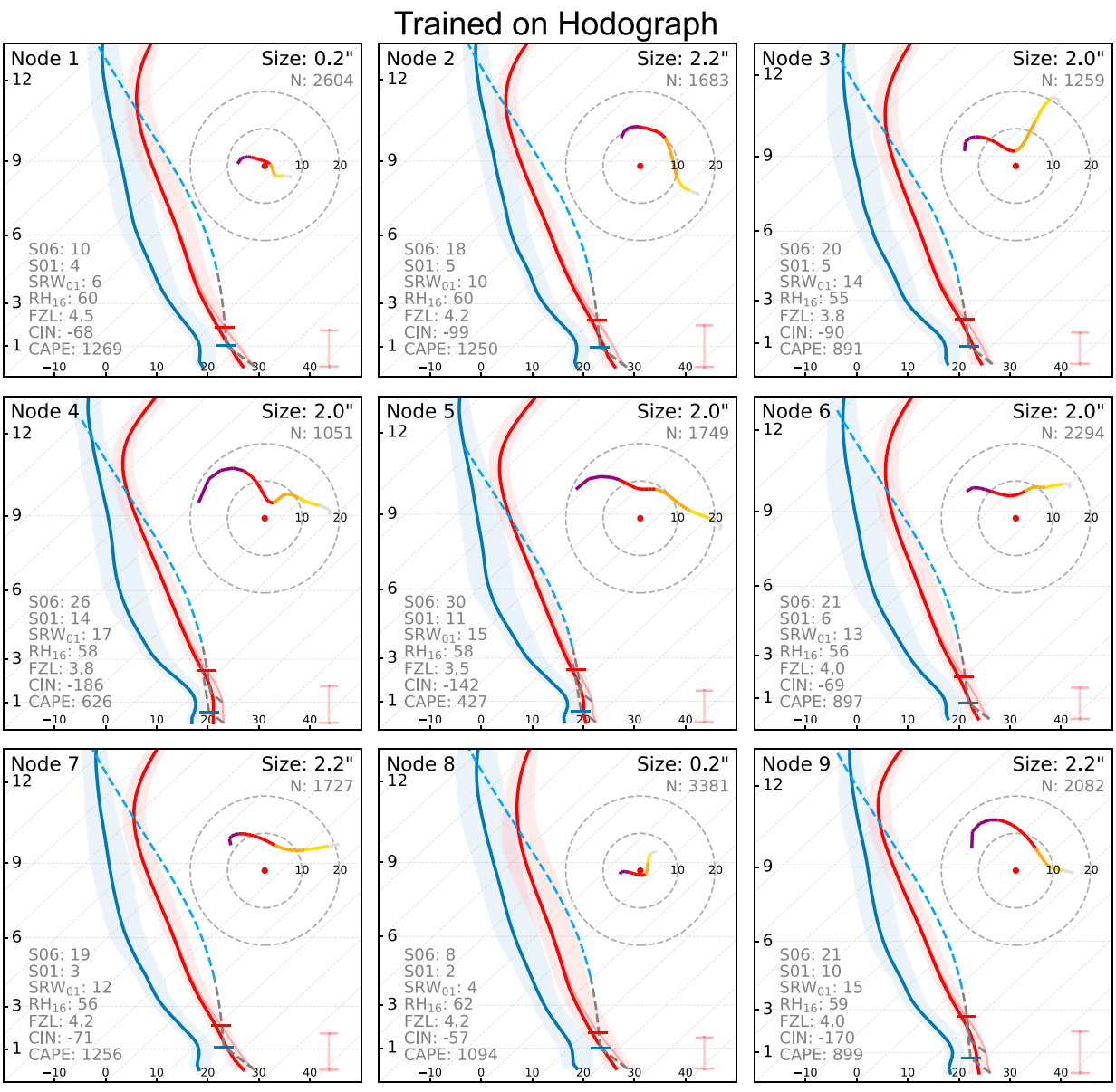

FIG. 2. As in Fig. 1, but the mean skew T and storm-relative hodograph for each node produced by a SOM given inputs of kinematic profiles for two hail size bins [smaller than 12.5 mm (0.5 in.), and at least 50 mm (2.0 in.)]. All composite hodographs are displayed relative to the estimated storm motion (Bunkers et al. 2000) calculated from the mean profile. The median hail size in each node is displayed on the top right, as is the number (N) of cases in each node. Various other aspects of the display are outlined in Fig. 1.

associated with greater CAPE and stronger S06 than smaller hail. Also similar to Johnson and Sugden (2014) and Nixon and Allen (2022), S06 varies little per hail size beyond 25 mm (1.0 in.). In other words, as hail size increases, the shear profile appears to become less able to distinguish between hail sizes. This is in contrast to CAPE, which increases continuously with hail size. Although this may initially suggest that the shear profile is less important than the thermodynamic profile in hail prediction [a conclusion drawn by Warren et al. (2021)], we choose to consider the alternate hypothesis, and investigate *how* wind shear regulates large hail potential.

Although examining the mean characteristics of hail environments can prove useful in operations (e.g., Johnson and Sugden 2014; Nixon and Allen 2022), this may mask important relationships between parameters that add complexity. As the physical processes that govern relationships, such as those between CAPE and shear, are unknown, we leverage the self-organizing map to separate out cases that may originate due to different environmental processes. We first consult a self-organizing map trained on all kinematic (u and v wind) profiles of hail of any size (Fig. 2). A variety of shear profiles were associated with sig.-severe hail, with strong variance between nodes, which included

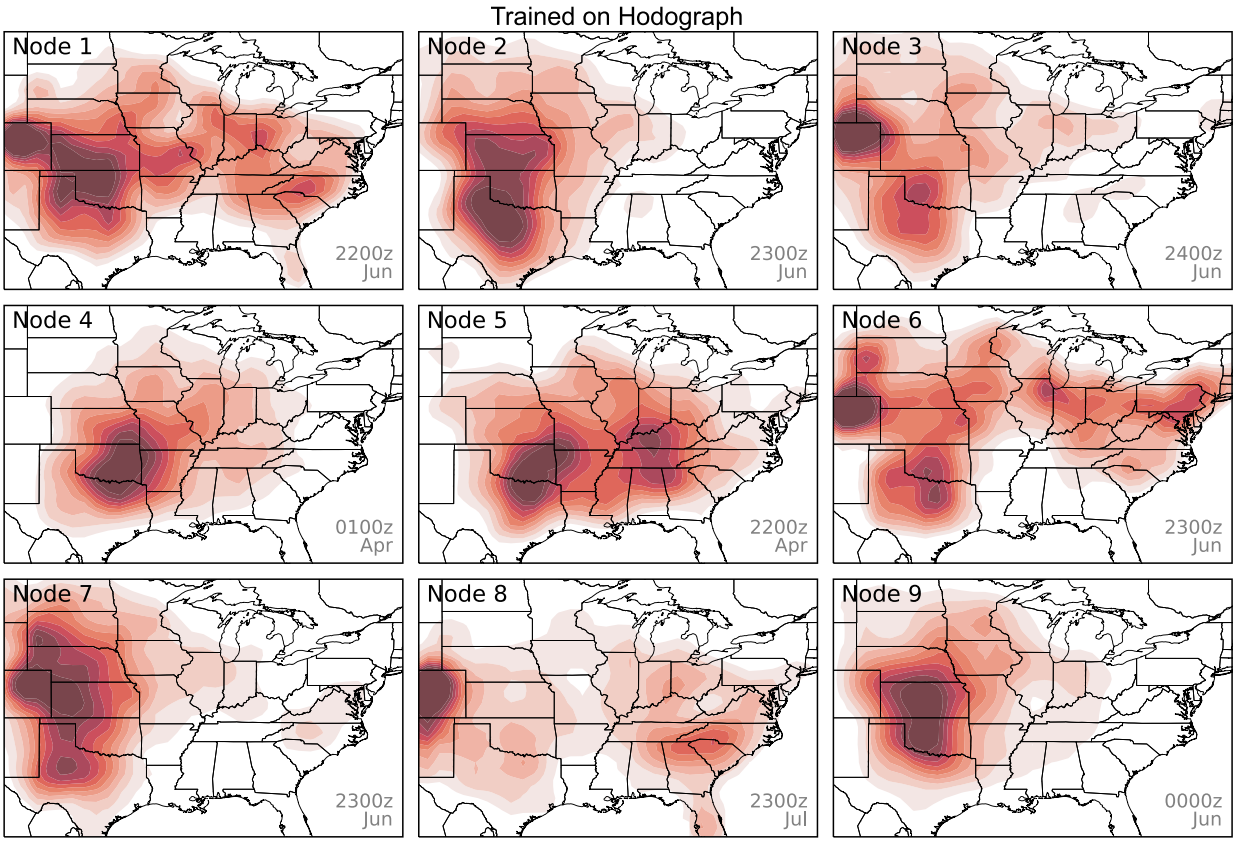

FIG. 3. 2D kernel density estimate of the locations of reports in each node produced by a SOM given inputs of kinematic profiles for two hail size bins [smaller than 12.5 mm (0.5 in.), and at least 50 mm (2.0 in.)]. The mean month and time of day for each node is also displayed, calculated using circular statistics (which account for ranges of values without a significant zero point, e.g., to ensure that the average of 2300 and 0100 UTC is 0000 UTC, not 1200 UTC).

veering, backing, and straight hodographs. However, the nodes with the weakest S06 (Nodes 1 and 8) were associated with a subsevere average hail size. In general, stronger S06 was associated with smaller CAPE, and weaker S06 was associated with larger CAPE. Stronger S01 (e.g., in Nodes 4, 5, and 9) was also accompanied by stronger CIN.

The prevalence of the various shear regimes varied across the central United States (Fig. 3). While nodes with weak S01 were found especially in the southern and central High Plains (and associated with deeper mixed layers per Fig. 2), the nodes with the strongest S01 (Nodes 4, 5, and 9) were found especially from the southern plains into the Ohio River valley. The shear profiles varied considerably by time of day and month, such that seasonal variability and the diurnal cycle were likely important in each regime. The cases with the strongest S06 were most common in April, while the cases with the weakest S06 were more common in June and July.

In contrast, a self-organizing map trained on only the T and w profiles shows that while a variety of temperature and moisture profiles are conducive to hail, some dependencies may exist (Fig. 4). A variety of CAPE and moisture profiles were associated with sig.-severe hail, but profiles with drier mid and upper-level air (Nodes 1, 3, and 6) were accompanied by stronger CAPE. The profiles with the weakest CAPE (Nodes 2, 5, 7, and 9) were accompanied by the lowest FZLs, and stronger S06 (especially for sig.-severe hail cases).

The various thermodynamic regimes also exhibited differences in frequency by region (Fig. 5). Drier profiles (e.g., Nodes 1, 3, and 6) were generally confined to the central and southern plains and High Plains. Profiles with higher relative humidity through a deeper layer (e.g., Nodes 4, 5, and 8) extended into the Midwest. The shallowest CAPE profiles (e.g., Nodes 2 and 7) were found in the higher terrain around the Colorado Front Range. Compared to the clusters of kinematic profiles, the clusters of thermodynamic profiles were less sensitive to the time of day.

b. Deep-layer shear, CAPE, and relative humidity

As a first hypothesis, we investigate if larger hail is favored by a balance of wind shear, CAPE, and relative humidity. As explored above, the variance in the self-organizing maps may be a function of multiple potential relationships between these profiles. Though the SOMs were useful in revealing these, they are less helpful at isolating the impacts of each profile on hail growth. Consequently, we hereafter investigate each relationship separately. By subsetting cases based on

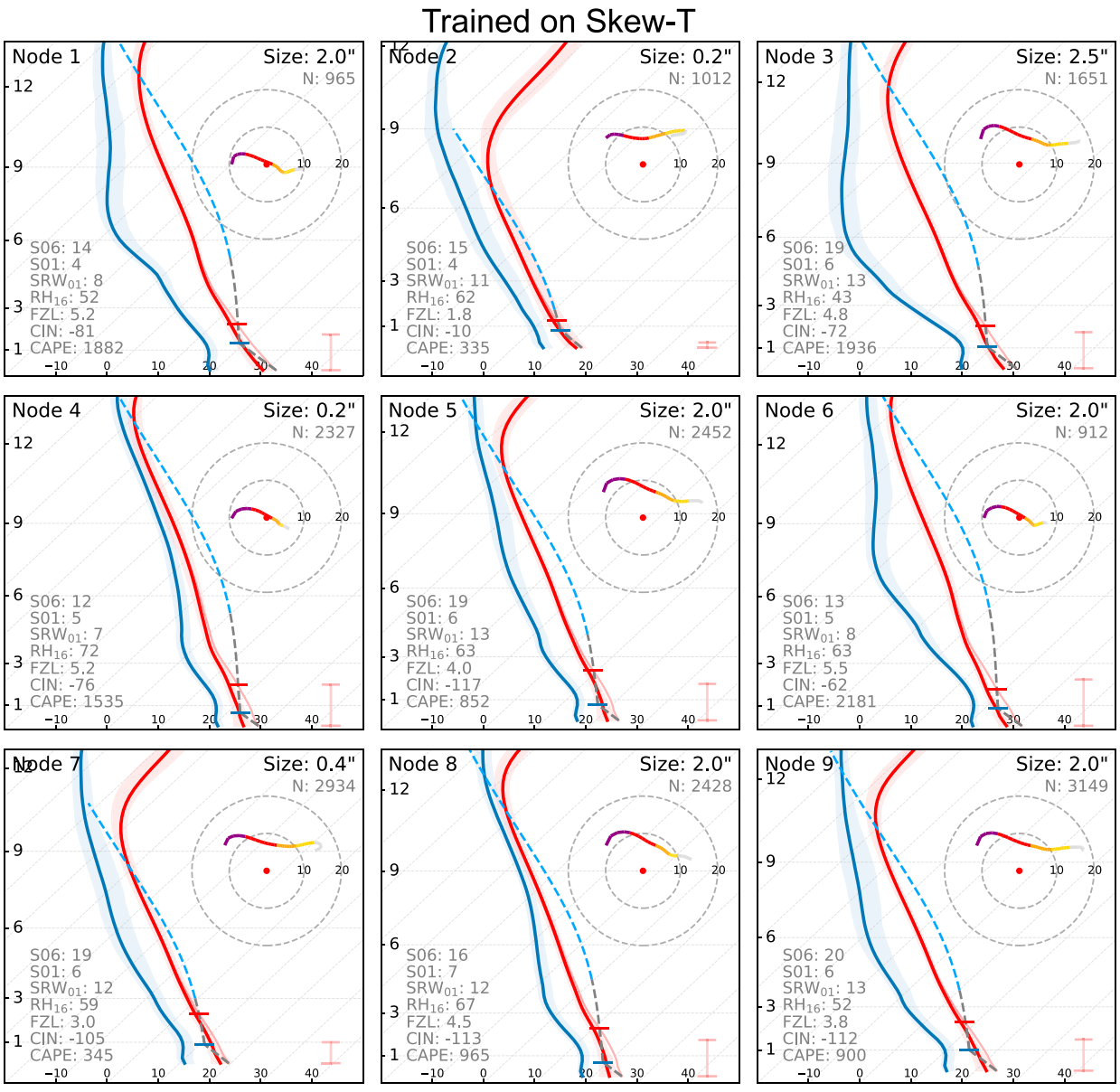

FIG. 4. As in Fig. 2, but for a SOM given inputs of thermodynamic profiles.

"low" and "high" thresholds of various environmental parameters, we can more directly examine their individual controls on hail potential, and any factors that may compensate for a change in another aspect of the profile.

The mean relationship between CAPE and S06 is illustrated in Figs. 6 and 7. In Fig. 6, weaker CAPE is accompanied by stronger S06 and a lower FZL. S06 is highest for sig.-severe hail in low CAPE. Differences in both S06 and FZL between the low CAPE and high CAPE sig.-severe hail samples are statistically significant at the 1% level using a Mann–Whitney U test (Mann and Whitney 1947). In Fig. 7, similar relationships are evident, with weaker S06 accompanied by stronger CAPE (even for smaller hail), and stronger S06 accompanied by a lower FZL. Stronger S06 is also associated with weaker CAPE and stronger CIN. Differences in CAPE, CIN, and FZL between the low S06 and high S06 sig.-severe hail samples are all statistically significant at the 1% level.

Since relative humidity of the ambient air also impacts the reduction of CAPE through entrainment, the relationship between CAPE and relative humidity in cases of sig.-severe hail is examined in Fig. 8. As RH13 decreases, the magnitude of CAPE favorable for sig.-severe hail increases substantially. The differences in CAPE between the low RH13 and high RH13 samples are statistically significant at the 1% level using a Mann–Whitney U test. This relationship is still notable in the 3–6-km layer, and even the 6–9-km layer (not shown).

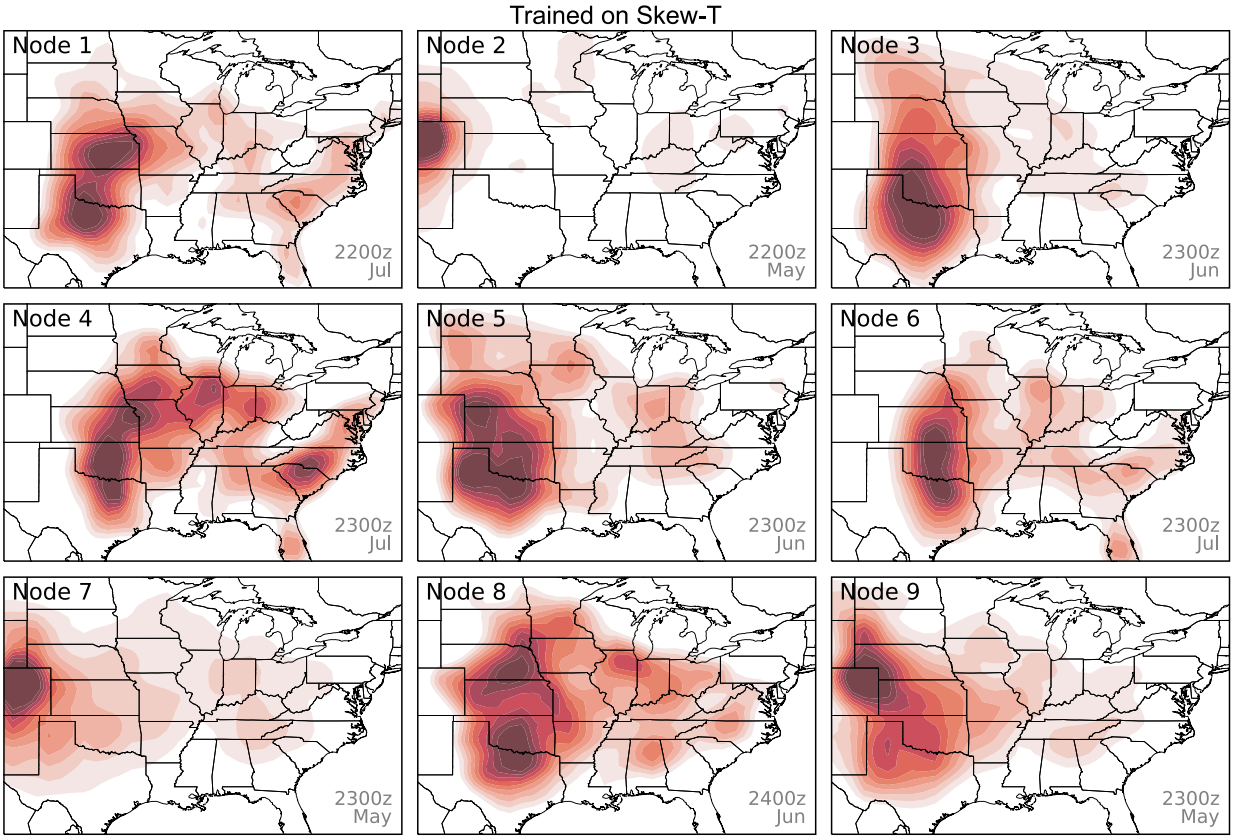

FIG. 5. As in Fig. 3, but for a SOM given inputs of thermodynamic profiles.

Since the entrainment of dry and stable air into an updraft may dilute its buoyancy (Peters et al. 2019, 2023), this result may be observational evidence of the impacts of entrainment on hail growth (or, perhaps, storm formation and maintenance).

The relationships shown in Figs. 1–4 suggest that hailstorms can form in a variety of combinations of CAPE, shear, and relative humidity. This is not surprising, since the net CAPE available to an updraft depends not only on the CAPE profile, but on the wind shear and relative humidity of the ambient environment (Peters et al. 2019, 2023). The relationship between these parameters in hail environments is illustrated in Fig. 9. Rather unsurprisingly, lower RH16 is accompanied by stronger CAPE and/or stronger S06. Likewise, weaker S06 is accompanied by stronger CAPE and/or higher RH16 (which may combat entrainment). On the other hand, the reverse is also true; stronger S06 paired with a moister troposphere is accompanied by weaker CAPE. This may be observational evidence that excess CAPE without entrainment may be detrimental to hail growth (Lin and Kumjian 2022). Rather, an "optimal" degree of entrainment-adjusted CAPE may exist that depends on wind shear and relative humidity.

c. *Low-level storm-relative winds and CAPE*

For the second hypothesis, we investigate excess low-level storm-relative winds as unfavorable for hail growth without compensation from the low-level buoyancy profile. As noted in simulations by Dennis and Kumjian (2017), Kumjian et al. (2021), and Lin and Kumjian (2022), in cases of strong low-level shear, strong low-level storm-relative winds can detrimentally affect the trajectories of hailstones through the hail growth zone. The thermodynamic profiles favorable for sig.-severe hail in high S01, high S06, and high SRW01 shear profiles are shown in Fig. 10 relative to an average shear profile (a "control" sample). Evidently, sig.-severe hail is still possible even with strong S01 [a conclusion also drawn from Kumjian et al. (2021) and Homeyer et al. (2023)] and SRW01. However, these cases are accompanied by weaker CAPE, stronger CIN, and a higher most-unstable LPL than average. The differences in CIN between these samples and the control sample are statistically significant at the 1% level using a Mann–Whitney U test. The buoyancy profile of the strong SRW01 sample is particularly different from the control sample, with stronger CIN, a higher LFC, and weaker sub-HGZ CAPE (statistically significant at the 1% level). On the other hand, the thermodynamic profiles favorable for sig.-severe hail in strong S06 without strong S01 or SRW01 are more similar to the average sample.

How do the favorable low-level shear profiles of hailstorms change with changes in the low-level buoyancy profile? To disentangle this question, the relationships between S01, SRW01, CIN, and LFC are explored in 2D histograms in Fig. 11. The relationship between S01 and the low-level thermodynamic profile is complicated; while increasing S01 is generally accompanied by

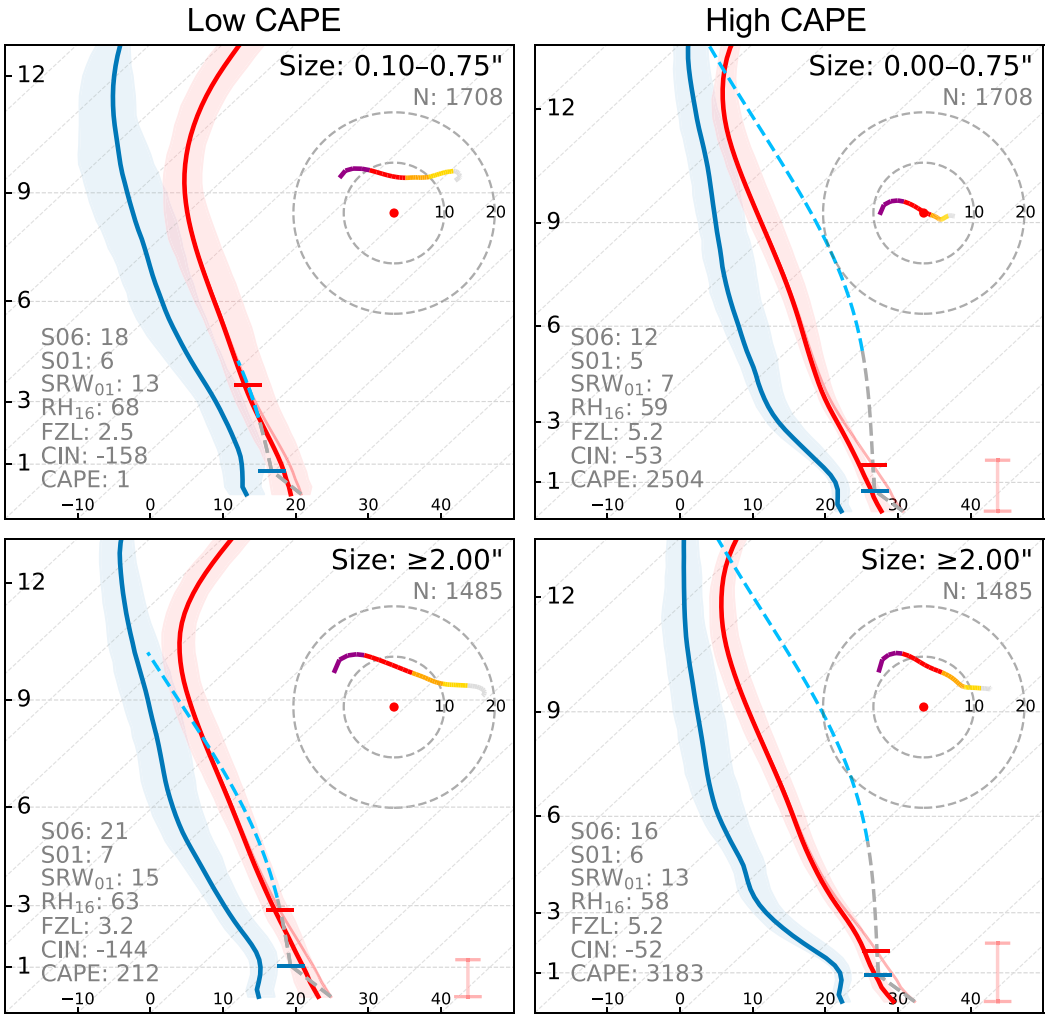

FIG. 6. As in Fig. 1, but the mean skew T and storm-relative hodograph for (top) hail smaller than 12.5 mm (0.5 in.), and (bottom) at least 50 mm (2.0 in.), only for cases with (left) low CAPE (CAPE less than the 15.9th percentile) and (right) high CAPE (CAPE greater than or equal to the 84.1st percentile). Although all cases with CAPE < 250 J kg^{-1} were removed prior to this analysis, some samples may still have mean CAPE < 250 J kg^{-1} because variables are calculated using the mean profile, not the mean across the sample.

increasing CIN (as showed above), this relationship is less clear when compared to the LFC. Furthermore, it is not known whether or not the increase in CIN with increasing S01 is simply a by-product of boundary layer decoupling beneath strong low-level flow (e.g., Mead and Thompson 2011), rather than a physically relevant consideration for hail potential. Conversely, the relationship between SRW01 and these parameters has no known codependency, yet is more consistent: stronger-than-average SRW01 is accompanied by both stronger CIN and a higher LFC, especially when S01 is weaker. Thus, the correlation between SRW01 and the low-level buoyancy profile may be meaningful to hail prediction.

What is the significance of stronger CIN or a higher LFC in cases of stronger low-level storm-relative winds? Since both low-level buoyancy and storm-relative winds affect the trajectories and residence time of hailstones within the hail growth zone (Dennis and Kumjian 2017; Kumjian et al. 2021; Lin and Kumjian 2022), we hypothesize that the favorable ranges of these parameters may differ depending on the height of the HGZ. In cases of sig.-severe hail subset by strong SRW01 (Fig. 12), a higher FZL is accompanied by stronger CIN and a higher LFC (such that CAPE below the HGZ is minimized). On the other hand, a lower FZL evidently need not be accompanied by strong CIN or a high LFC (perhaps because CAPE below the HGZ is already minimized). The differences in CIN between the low FZL and high FZL profiles are statistically significant at the 1% level using a Mann–Whitney U test. Thus, we have reason to hypothesize that the relationship between the favorable low-level storm-relative winds and buoyancy profiles of hailstorms depends also on the FZL.

The relationship between S01, SRW01, and sub-HGZ CAPE is shown in Fig. 13. Here, SRW01 is consistently correlated with

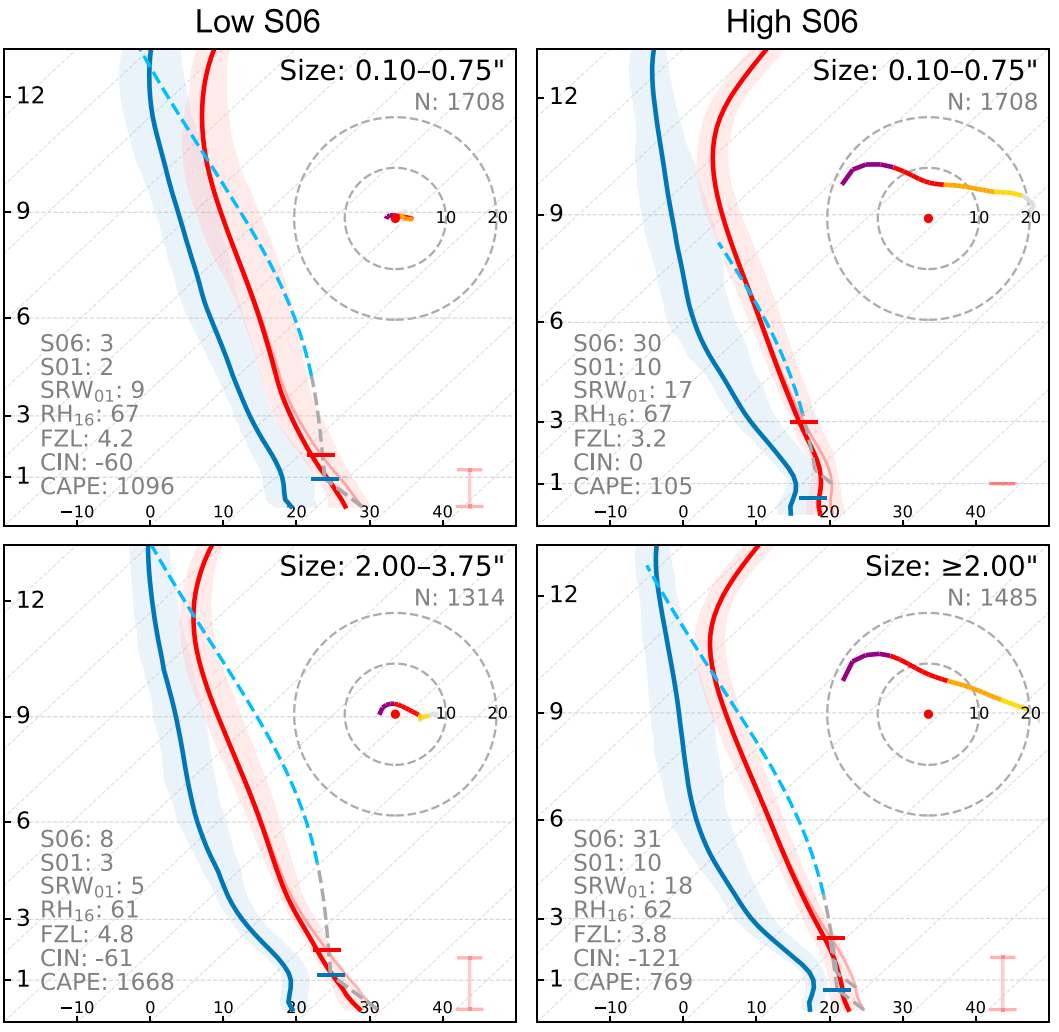

FIG. 7. As in Fig. 6, but only for cases with (left) low S06 and (right) high S06.

sub-HGZ CAPE, such that increasing SRW01 is met with decreasing sub-HGZ CAPE, regardless of S01. Likewise, the reverse relationship is also true: increasing sub-HGZ CAPE is met with decreasing SRW01. The full distribution of sub-HGZ CAPE for two subsets of the SRW01 parameter space are also shown via violin plots (Fig. 13). A difference in only 5 m s^{-1} (~10 kt) between samples is accompanied by a large shift in the favorable ranges of sub-HGZ CAPE (statistically significant at the 1% level using a Mann–Whitney *U* test). While weaker SRW01 is accompanied by a wide range of CAPE magnitudes, stronger SRW01 is skewed toward weaker sub-HGZ CAPE. The reverse relationship was similar (not shown), where stronger sub-HGZ CAPE was skewed toward weaker SRW01. Given these results, we find evidence that in environments with stronger low-level storm-relative winds, large hail is more likely with weaker sub-HGZ CAPE. Likewise, in environments with stronger sub-HGZ CAPE, large hail is more likely with weaker low-level storm-relative winds.

A SOM of the variety of buoyancy profiles favorable for large hail in strong SRW01 is shown in Fig. 14. In this sample, regardless of S01 and for all hail sizes, hail is produced in environments with weaker than average sub-HGZ CAPE. However, this is possible in a variety of different thermodynamic regimes. For instance, Nodes 1, 4, and 5 feature elevated effective inflow bases (Thompson et al. 2007). Elevated storms have often been noted to produce severe hail (Colman 1990; Horgan et al. 2007; Corfidi et al. 2008), and elevated EIBs are found in over 12% of all cases of severe hail in this dataset. Nodes 3, 7, and 9, while not elevated as defined by Thompson et al. (2007), feature an elevated most-unstable LPL. The nodes with the least surface-based CIN (Nodes 6 and 8) have the highest surface elevations. Thus, large hail is possible even with strong low-level storm-relative winds, but most of these cases feature either elevated buoyancy profiles or an otherwise low FZL.

d. Storm depth and freezing level

Finally, we investigate the role of storm depth on hail growth. Although depth can be defined in several ways, the most-unstable MPL is used here to approximate the maximum potential height that an updraft can reach above the EL. Given

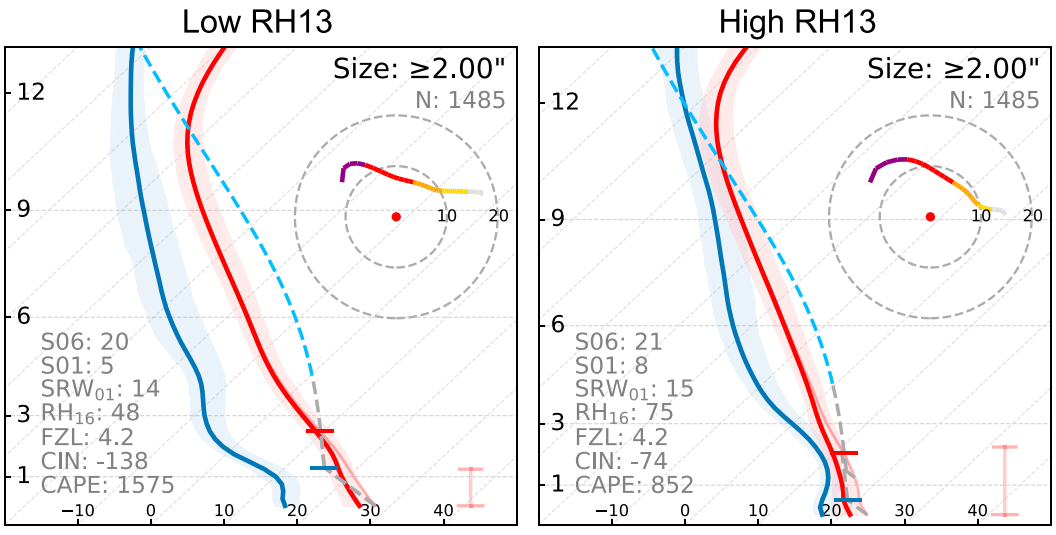

FIG. 8. As in Fig. 6, but the mean skew T and storm-relative hodograph for hail of at least 50 mm (2.0 in.), only for cases with (left) low RH13 (mean relative humidity from 1 to 3 km) and (right) high RH13.

previous studies (e.g., Nelson 1983; Browning and Foote 1976; Miller et al. 1988; Knight and Knight 2001), hail growth is not possible if an updraft fails to extend into sufficiently cold temperatures. The ability of an updraft to reach these optimal temperatures depends on two factors: the height of the FZL, and the depth of the storm. In Fig. 15, when the MPL is varied, we find that a shallower storm depth must be accompanied by a lower FZL. The differences in FZL heights between the low MPL and high MPL samples are statistically significant at the 1% level using a Mann–Whitney U test.

The extent to which potential storm depth (particularly above the freezing level) may affect maximum expected hail size is examined in more detail here. Past studies have noted that overshooting top height can serve as a reliable indicator for large hail potential in midlatitudes (Homeyer and Kumjian 2015; Murillo and Homeyer 2019). In Fig. 16, two relevant relationships can be seen. First, as MPL lowers (or as maximum potential storm depth becomes shallower), the mean FZL height for each size bin also lowers. In other words, though hail is possible with a variety of storm depths, these storms must have sufficient depth above the FZL to produce large hail. This result supports Zhou et al. (2021), who found that several different types of buoyancy profiles were associated with severe hail, but weaker and shallower buoyancy was most often found with a lower FZL.

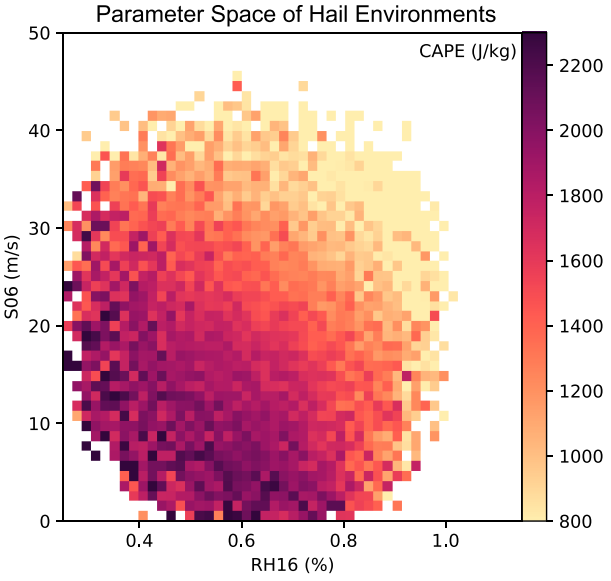

FIG. 9. 2D histogram of S06 and RH16 for all hail reports, colored by mean CAPE. Bins with less than four cases are omitted to reduce noise.

We acknowledge that CAPE and storm depth are ultimately correlated with the temperature profile through latent heat release, such that environments with higher FZLs generally feature more moisture and stronger CAPE. However, this correlation strongly depends on the lapse rate of temperature between the surface and the FZL, which may vary considerably per hail environment as shown throughout. Thus, although we acknowledge that the change in average FZL per MPL may be due in part to this correlation, we argue that there is also a fundamental reason why a shallower storm must have a lower FZL to produce hail [i.e., to reach sufficiently deep into the HGZ (Nelson 1983; Browning and Foote 1976; Miller et al. 1988; Knight and Knight 2001)].

Second, and more importantly for the sake of hail size forecasting, is that MPL serves as a limiting factor on maximum potential hail size. In Fig. 16, although large hail is possible with a variety of storm depths, increasingly larger hail is distinctly limited to increasingly higher MPLs. In other words, deeper storms can produce larger hail, as has been noted in remote sensing studies (Homeyer and Kumjian 2015; Murillo and Homeyer 2019). When all unique observed hail sizes are compared to the lowest MPL for each size, they are correlated with a Pearson correlation of 0.49, significant at the 1% level using a Student's t

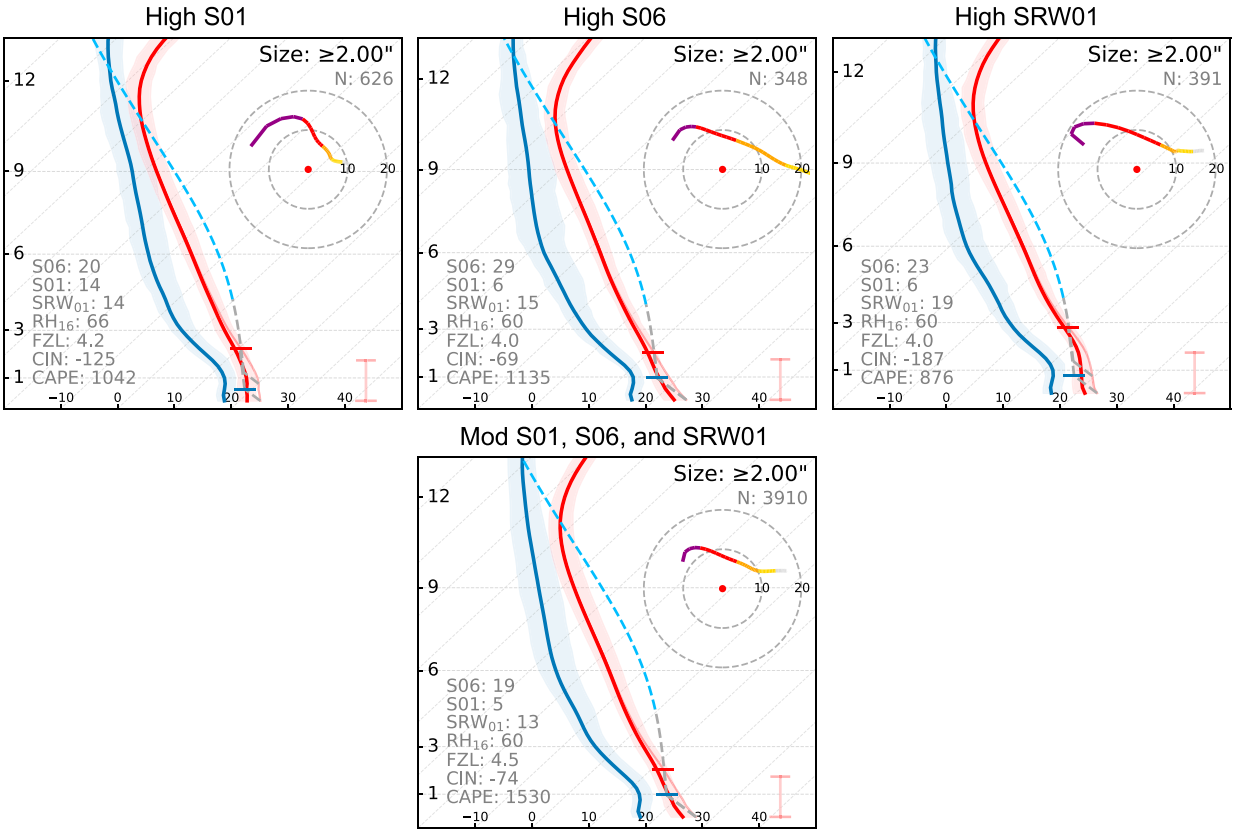

FIG. 10. As in Fig. 6, but the mean skew T and storm-relative hodograph for hail of at least 50 mm (2.0 in.), only for cases with (top left) moderate (defined as within one standard deviation from the mean) S06 and SRW01 but high S01; (top center) moderate S01 and SRW01 but high S06; (top right) moderate S01 and S06 but high SRW01; and (bottom) moderate S01, S06, and SRW01.

test. Neither CAPE nor HGZ CAPE displays a similar relationship in Fig. 16, despite their more prevalent use in hail size forecasting, echoing past studies (Brooks 2013; Sherburn and Parker 2014; Taszarek et al. 2020). Although this may be related to how the bounds of the HGZ have been defined in previous studies (e.g., perhaps from −30° to −10°C is not ideal), we find evidence that estimations of storm depth may better serve hail size prediction than estimations of buoyancy.

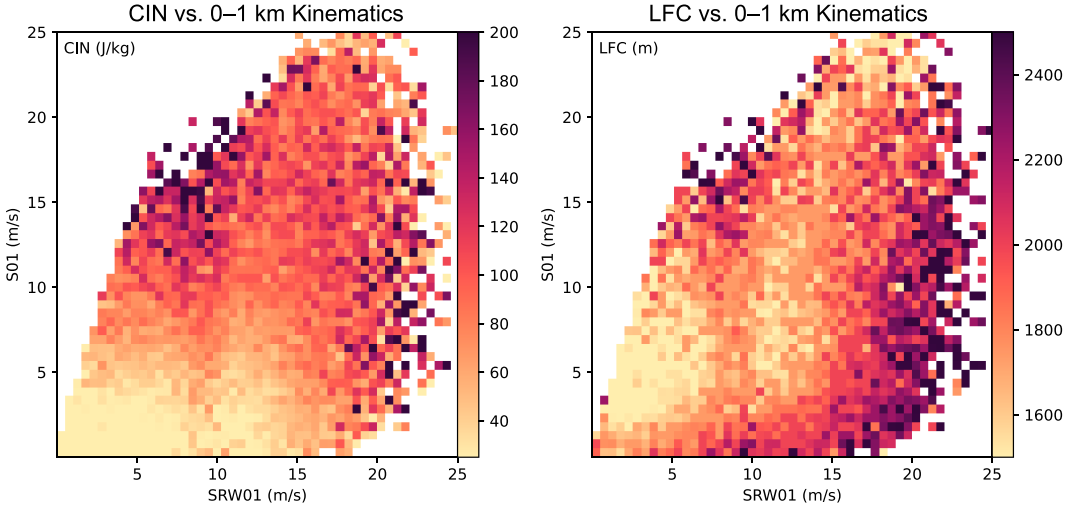

FIG. 11. As in Fig. 9, but 2D histograms of S01 and SRW01 for all hail reports, colored by (left) CIN and (right) LFC. Bins with less than four cases are omitted to reduce noise.

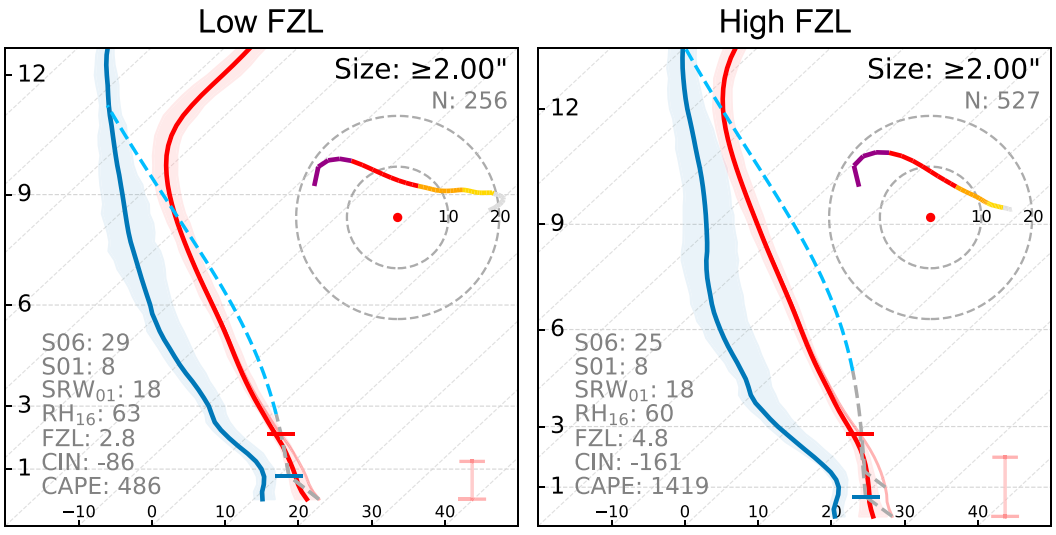

FIG. 12. As in Fig. 6, but the mean skew T and storm-relative hodograph for hail of at least 50 mm (2.0 in.), only for cases with a high mean 0–1-km storm-relative wind and (left) low FZL and (right) high FZL.

4. Summary and discussion

To summarize the key findings of this analysis, the environments of large hail appear to depend on the following relationships:

1) Favorable wind shear, CAPE, and relative humidity:
   - Favorable CAPE values depend on deep-layer shear and relative humidity, presumably as a function of entrainment.
   - An entrainment-adjusted CAPE may be useful in hail forecasting.
2) Favorable storm-relative winds and CAPE below the hail growth zone
   - Strong low-level storm-relative winds are unfavorable for large hail, unless CAPE below the HGZ is sufficiently weak.
   - Strong CAPE below the HGZ is unfavorable for large hail, unless low-level storm-relative winds are sufficiently weak.
3) Sufficient storm depth into favorable temperatures:
   - Lower freezing levels support large hail more readily, even with shallower buoyancy, stronger low-level CAPE, or stronger storm-relative winds.
   - Storm depth (particularly in/above the freezing level), rather than CAPE, may be useful in forecasting maximum potential hail size.

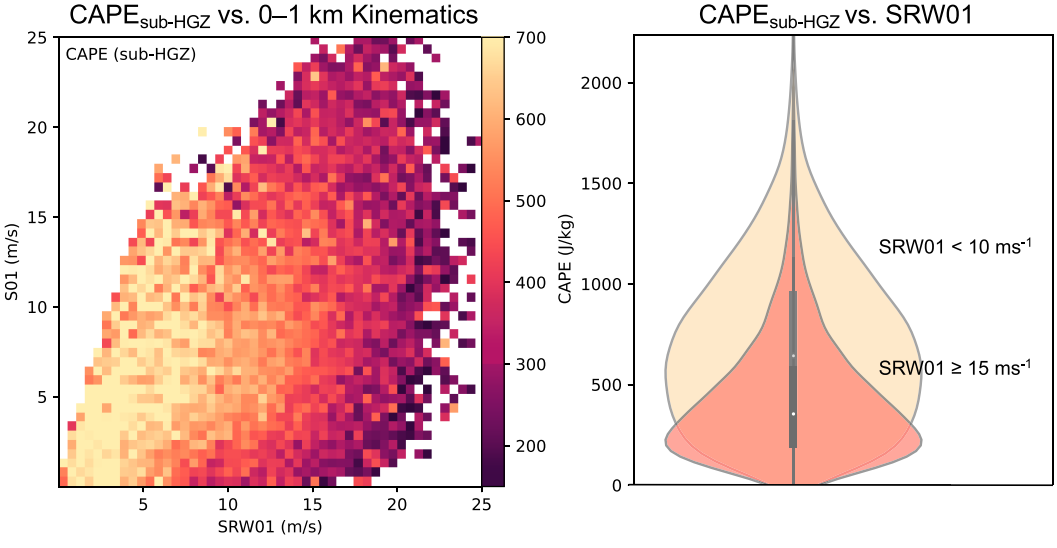

FIG. 13. (left) As in Fig. 11, but 2D histograms of S01 and SRW01 for all hail reports, colored by LFC-FZL. Bins with less than four cases are omitted to reduce noise. (right) A violin plot of the distribution of FZL-LFC for two subsets of cases: SRW01 < 10 m s^{-1} and SRW01 ≥ 10 m s^{-1}.

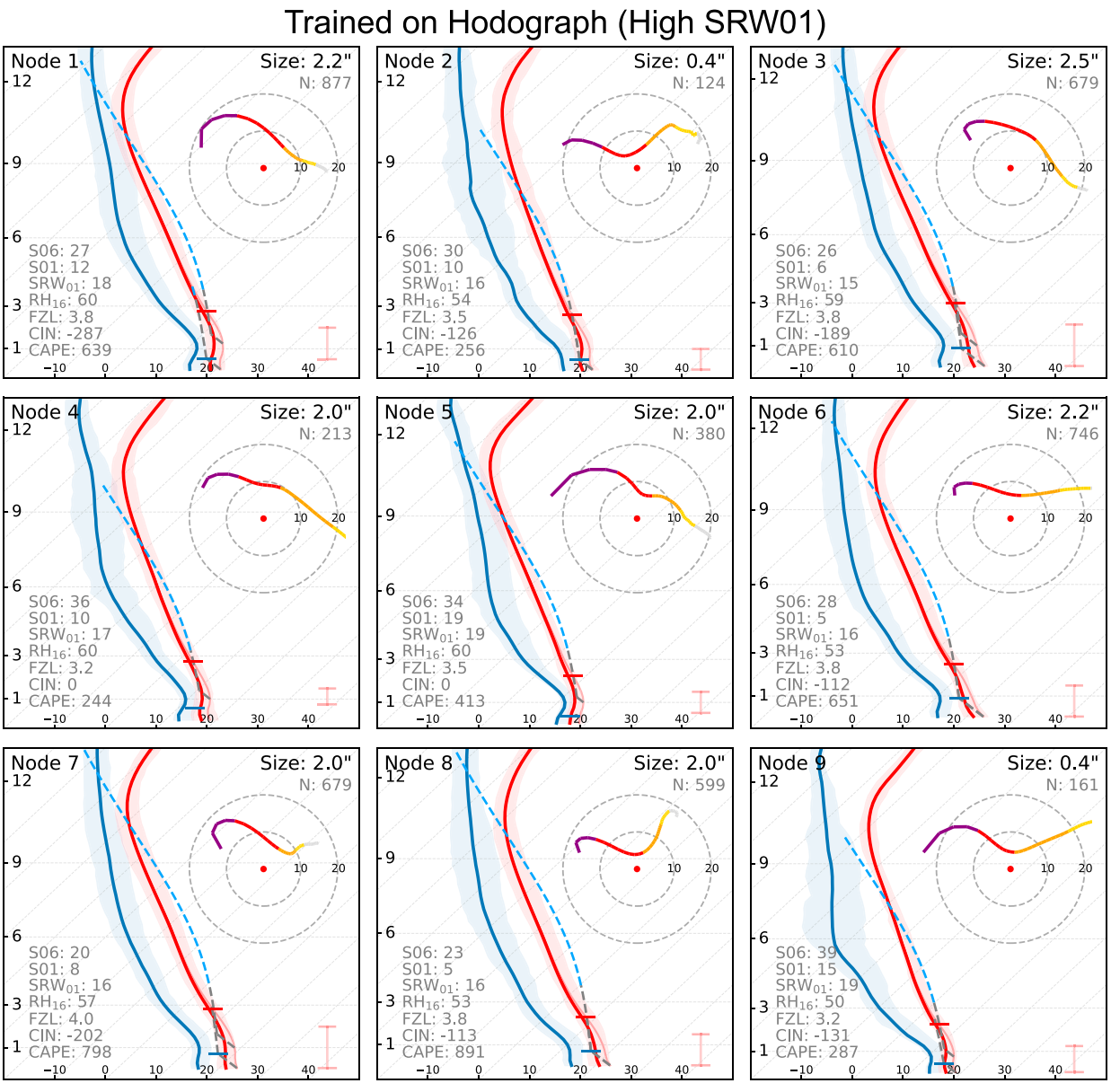

FIG. 14. As in Fig. 2, but for a SOM given inputs of kinematic profiles, only for cases with SRW01 at or above the 75th percentile. Although all cases with CAPE < 250 J kg^{-1} were removed prior to this analysis, some samples may still have mean CAPE < 250 J kg^{-1} because variables are calculated using the mean profile, not the mean across the sample.

This study finds that hail growth is a multivariate problem affected by multiple factors. The relevant parameters and physical relationships involved in these factors are found to be very different than those consulted traditionally in severe weather forecasting. The three main facets examined herein are explored below.

First, large hail environments appear to depend on a favorable combination of CAPE, deep-layer shear, and deep-layer relative humidity. Though the concept and ramifications of entrainment (Peters et al. 2020a) and condensate loading (Storer and Van den Heever 2013) are becoming more prevalent in literature, our current parameter-based workflow does not yet account for these in CAPE estimations. However, this study shows that CAPE, deep-layer shear, and deep-layer relative humidity all appear intertwined, such that deficits in one can be compensated by excesses in another in cases of large hail. This strongly suggests that entrainment-based adjustments to traditional calculations of CAPE (i.e., Peters et al. 2020a) may add value for hail prediction.

Second, large hail environments appear to depend on a favorable balance between storm-relative winds and buoyancy below the hail growth zone. Although stronger storm-relative inflow can sustain larger storms (Peters et al. 2020b) that

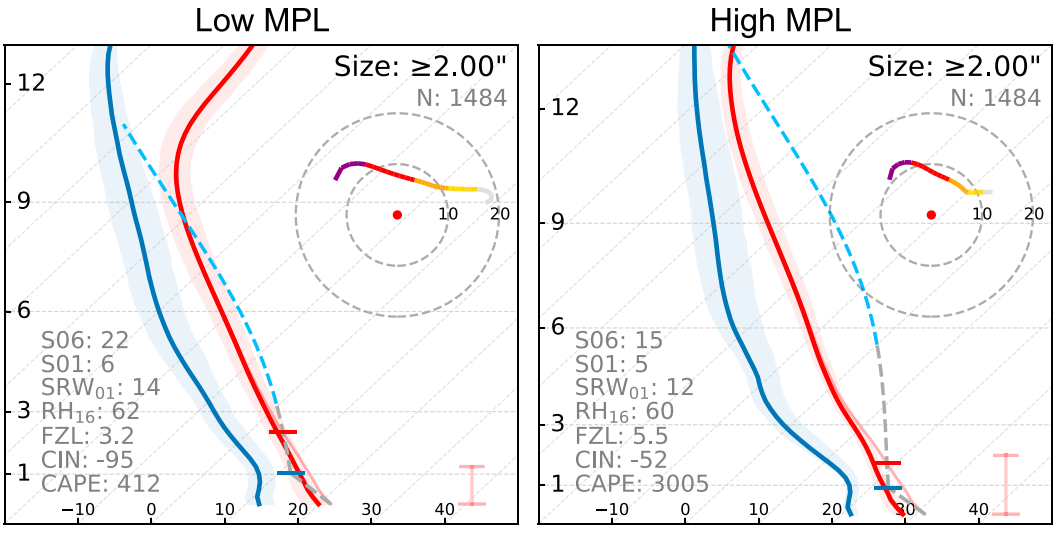

FIG. 15. As in Fig. 6, but the mean skew T and storm-relative hodograph for hail of at least 50 mm (2.0 in.), only for cases with (left) low MPL and (right) high MPL.

produce more hail mass (Dennis and Kumjian 2017; Homeyer et al. 2023), excess low-level storm-relative winds have been found to inhibit hail growth (Dennis and Kumjian 2017; Lin and Kumjian 2022; Kumjian et al. 2021). Likewise, excess low-level buoyancy may have similar impacts (Lin and Kumjian 2022). This study finds evidence that large hail is common even with strong low-level storm-relative winds, but that these environments are accompanied by weaker-than-average buoyancy below the hail growth zone. Likewise, environments with stronger buoyancy below the hail growth zone are accompanied by weaker low-level storm-relative winds. Though the physical reasons for this compensation are beyond the scope of this paper, we speculate that the higher the FZL, the more time an ascending air parcel has to be acted upon by the storm-relative wind, and thus the more momentum it will have once it reaches the hail growth zone [and the less residence time it will have within it, as explored in Lin and Kumjian (2022)]. In this way, if low-level storm-relative winds are stronger, a hailstorm may benefit

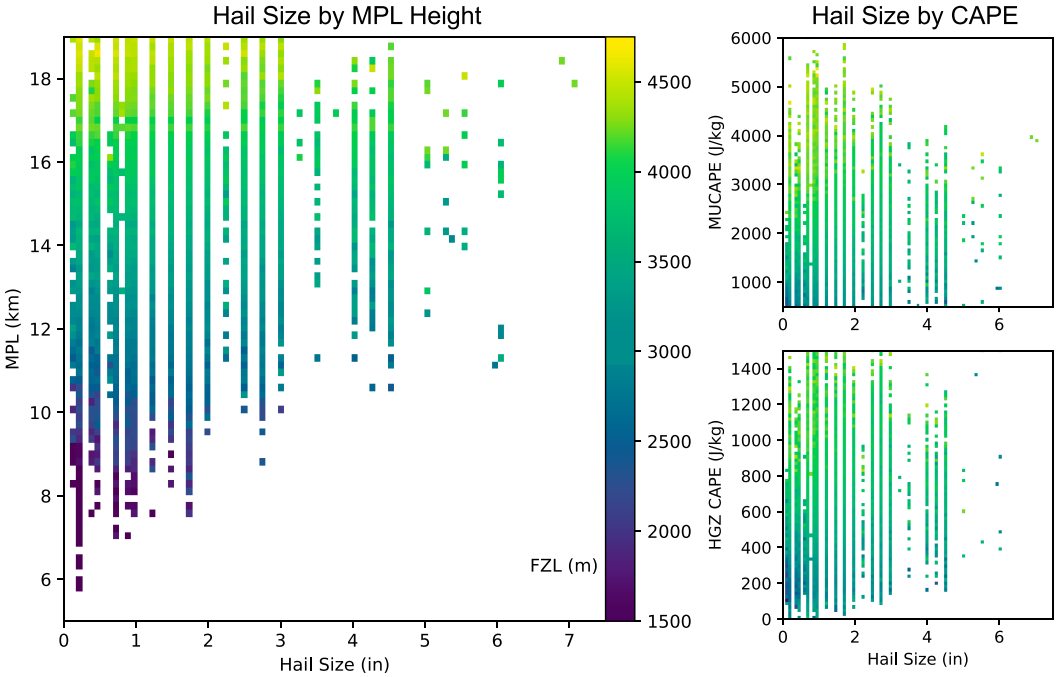

FIG. 16. As in Fig. 9, but 2D histograms of (left) MPL and hail size; (top right) MUCAPE and hail size; and (bottom right) HGZ CAPE and hail size, for all hail reports, colored by mean FZL.

from a higher level of free convection. This may explain the prevalence of cases with elevated inflow bases, which account for over 12% of severe hail reports in this study. More research through simulations may be necessary to better understand how parcel trajectories through the hail growth zone are modulated by low-level CAPE.

Third, parameterizations of storm depth, especially with respect to the hail growth zone, may be critical in hail prediction. Although CAPE is more commonly used in forecasting, we find that the MPL serves as a more robust limiting factor for hail size, such that deeper storms can produce larger hail [which reflects the utility of overshooting top height in large hail detection (Homeyer and Kumjian 2015; Bedka et al. 2018; Bang and Cecil 2019; Murillo and Homeyer 2019)]. In other words, it may matter less how much CAPE exists in a vertical profile, and more how deep a storm can potentially become in that profile. We also find that shallower storms are associated with lower FZLs, a result also found by Zhou et al. (2021). Future work may seek to better understand the controls of CAPE and storm depth on hail size, and to gain more clarity on whether a storm's depth above the FZL, or total depth, would be a more skillful predictor of hail size. Investigations of storms producing large accumulations of small hail (Kumjian et al. 2019) may also consider the possibility that shallower storms limit maximum hail size.

These controls may provide new insights into the climatology of large hail. For instance, in the United States, hail is common in the Great Plains, yet comparatively infrequent east of the Mississippi River (Allen and Tippett 2015; Allen et al. 2017; Elmore et al. 2022). A number of environmental factors may influence this. First, a higher surface elevation typically means a lower FZL. Given the sensitivity of large hail to FZL as explored above, this may explain the prevalence of large hail in the High Plains and the Appalachian Mountains (Allen and Tippett 2015), as well as the Alps in Europe (Púčik et al. 2019). These results corroborate those found by Zhou et al. (2021), who found a variety of different thermodynamic profiles to be favorable for large hail, including cases with low FZLs. Second, the prevailing shear profiles for severe weather episodes change across the country. Events in the Southeast United States are often accompanied by strong synoptic low-level flow *and* a warm, buoyant marine boundary layer, a combination that may limit hail production [this is supported by observations (Murillo et al. 2021)]. Although events in the central Great Plains are also often accompanied by a diurnally driven low-level jet (Bonner 1968), nocturnal cooling during the early evening transition may serve to limit surface-based convection, but allow elevated storms (Colman 1990; Horgan et al. 2007; Corfidi et al. 2008) that are more apt to produce severe hail. In contrast, events in the High Plains are generally removed from the influence of the diurnal low-level jet (Bonner 1968), thus perhaps more apt to produce severe hail even with stronger low-level buoyancy.

How can these results inform operational forecasting? The understanding of hail environments has evolved rapidly over the past decade. Evidence from this (and previous) research propose several new approaches to the prediction of large hail. First, an entrainment-adjusted CAPE (Peters et al. 2023) may aid forecasters in assessing whether CAPE is "optimal" for large hail. Second, an analysis of low-level storm-relative winds and CAPE below the hail growth zone may be critical in distinguishing between environments that can and cannot support large hail. Third, an assessment of potential storm depth, particularly above the freezing level, may support more informed predictions of maximum potential hail size.

While forecasters may favor the simplicity of parameters, this study challenges those currently used in hail forecasting. Though variables such as CAPE, lapse rates, FZL, and bulk shear show apparent statistical significance in prior studies (e.g., Johnson and Sugden 2014; Storm Prediction Center 2019), we argue that these may be merely proxies for more relevant quantities. For instance, extreme CAPE (often thought to be conducive to giant hail) may simply be a proxy for particularly deep convection. This study finds that maximum potential hail size is more directly impacted by MPL than CAPE. Steep lapse rates (also a rule of thumb for large hail environments) may simply serve as a proxy for strong CAPE and a low FZL. Although steep lapse rates accompany large hail in the United States (Johnson and Sugden 2014), comparable lapse rates are less prevalent in other regions (Taszarek et al. 2021a; Zhou et al. 2021). The FZL itself may serve more than one purpose; while low FZLs are traditionally thought to reduce the amount of time a hailstone has to melt, we argue that its role as a proxy for the hail growth zone may be just as important.

Although emphasis in forecasting is placed on the background environment, we remind the reader that the characteristics of the storm itself, and any storm interactions, may also heavily influence potential hail size. Similarly to the buoyancy problem, a storm's propensity to produce large hail is primarily regulated by its structure and intensity, regardless of how these characteristics were attained.

Acknowledgments. We would like to acknowledge Matthew Kumjian for his extensive feedback and guidance. This research was based upon work supported by the National Science Foundation under Grant AGS-1855054. This research was supported by the Earth and Ecosystem Science PhD program at Central Michigan University, and by a grant from the Polish National Science Centre Grant 2020/39/D/ST10/00768.

Data availability statement. Data used in this paper were derived from the ERA5 reanalysis (openly available through the Climate Data Source at https://cds.climate.copernicus.eu/#!/home), storm reports from the Storm Prediction Center (https://www.spc.noaa.gov/wcm/data/1955-2021_hail.csv.zip, CoCoRaHS (https://www.cocorahs.org/viewdata/), and MPING (available for research with licensing at https://mping.ou.edu/static/mping/access.html). The authors' post-processed ERA5 dataset of quality controlled hail cases, with latitude, longitude, time, hail size, and environmental variables are available upon request. The associated 1D vertical profile of standard ERA5 data are available from the authors upon request due to dataset size, but can be replicated using the location data within the postprocessed dataset and the ERA5 data from the Climate Data Store.

REFERENCES

Allen, J. T., and D. J. Karoly, 2014: A climatology of Australian severe thunderstorm environments 1979–2011: Inter-annual variability and ENSO influence. *Int. J. Climatol.*, **34**, 81–97, https://doi.org/10.1002/joc.3667.

——, and M. K. Tippett, 2015: The characteristics of United States hail reports: 1955–2014. *Electron. J. Severe Storms Meteor.*, **10** (3), https://doi.org/10.55599/ejssm.v10i3.60.

——, ——, and A. H. Sobel, 2015: An empirical model relating U.S. monthly hail occurrence to large-scale meteorological environment. *J. Adv. Model. Earth Syst.*, **7**, 226–243, https://doi.org/10.1002/2014MS000397.

——, ——, Y. Kaheil, A. H. Sobel, C. Lepore, S. Nong, and A. Muehlbauer, 2017: An extreme value model for U.S. hail size. *Mon. Wea. Rev.*, **145**, 4501–4519, https://doi.org/10.1175/MWR-D-17-0119.1.

——, I. M. Giammanco, M. R. Kumjian, H. Jurgen Punge, Q. Zhang, P. Groenemeijer, M. Kunz, and K. Ortega, 2020: Understanding hail in the Earth system. *Rev. Geophys.*, **58**, e2019RG000665, https://doi.org/10.1029/2019RG000665.

Amburn, S. A., and P. L. Wolf, 1997: VIL density as a hail indicator. *Wea. Forecasting*, **12**, 473–478, https://doi.org/10.1175/1520-0434(1997)012<0473:VDAAHI>2.0.CO;2.

Anderson-Frey, A. K., Y. P. Richardson, A. R. Dean, R. L. Thompson, and B. T. Smith, 2017: Self-organizing maps for the investigation of tornadic near-storm environments. *Wea. Forecasting*, **32**, 1467–1475, https://doi.org/10.1175/WAF-D-17-0034.1.

Ashley, W. S., A. J. Krmenec, and R. Schwantes, 2008: Vulnerability due to nocturnal tornadoes. *Wea. Forecasting*, **23**, 795–807, https://doi.org/10.1175/2008WAF2222132.1.

Bang, S. D., and D. J. Cecil, 2019: Constructing a multifrequency passive microwave hail retrieval and climatology in the GPM domain. *J. Appl. Meteor. Climatol.*, **58**, 1889–1904, https://doi.org/10.1175/JAMC-D-19-0042.1.

Baumgardt, D., 2011: Hail estimation: How good are your spotters? 24 pp., https://www.weather.gov/media/arx/research/hail_size_MSP.pdf.

Bedka, K. M., J. T. Allen, H. J. Punge, M. Kunz, and D. Simanovic, 2018: A long-term overshooting convective cloud-top detection database over Australia derived from MTSAT Japanese advanced meteorological imager observations. *J. Appl. Meteor. Climatol.*, **57**, 937–951, https://doi.org/10.1175/JAMC-D-17-0056.1.

Blair, S. F., and J. W. Leighton, 2012: Creating high-resolution hail datasets using social media and post-storm ground surveys. *Electron. J. Oper. Meteor.*, **13**, 32–45, http://nwafiles.nwas.org/ej/pdf/2012-EJ3.pdf.

——, and Coauthors, 2017: High-resolution hail observations: Implications for NWS warning operations. *Wea. Forecasting*, **32**, 1101–1119, https://doi.org/10.1175/WAF-D-16-0203.1.

Bonner, W. D., 1968: Climatology of the low level jet. *Mon. Wea. Rev.*, **96**, 833–850, https://doi.org/10.1175/1520-0493(1968)096<0833:COTLLJ>2.0.CO;2.

Brimelow, J. C., G. W. Reuter, and E. R. Poolman, 2002: Modeling maximum hail size in Alberta thunderstorms. *Wea. Forecasting*, **17**, 1048–1062, https://doi.org/10.1175/1520-0434(2002)017<1048:MMHSIA>2.0.CO;2.

Brooks, H. E., 2009: Proximity soundings for severe convection for Europe and the United States from reanalysis data. *Atmos. Res.*, **93**, 546–553, https://doi.org/10.1016/j.atmosres.2008.10.005.

——, 2013: Severe thunderstorms and climate change. *Atmos. Res.*, **123**, 129–138, https://doi.org/10.1016/j.atmosres.2012.04.002.

——, J. W. Lee, and J. P. Craven, 2003: The spatial distribution of severe thunderstorm and tornado environments from global reanalysis data. *Atmos. Res.*, **67–68**, 73–94, https://doi.org/10.1016/S0169-8095(03)00045-0.

Browning, K. A., and G. B. Foote, 1976: Airflow and hail growth in supercell storms and some implications for hail suppression. *Quart. J. Roy. Meteor. Soc.*, **102**, 499–533, https://doi.org/10.1002/qj.49710243303.

Bunkers, M. J., B. A. Klimowski, J. W. Zeitler, R. L. Thompson, and M. L. Weisman, 2000: Predicting supercell motion using a new hodograph technique. *Wea. Forecasting*, **15**, 61–79, https://doi.org/10.1175/1520-0434(2000)015<0061:PSMUAN>2.0.CO;2.

Chase, R. J., D. R. Harrison, G. M. Lackmann, and A. McGovern, 2023: A machine learning tutorial for operational meteorology. Part II: Neural networks and deep learning. *Wea. Forecasting*, **38**, 1271–1293, https://doi.org/10.1175/WAF-D-22-0187.1.

Coffer, B. E., M. Taszarek, and M. D. Parker, 2020: Near-ground wind profiles of tornadic and nontornadic environments in the United States and Europe from ERA5 reanalyses. *Wea. Forecasting*, **35**, 2621–2638, https://doi.org/10.1175/WAF-D-20-0153.1.

Colman, B. R., 1990: Thunderstorms above frontal surfaces in environments without positive CAPE. Part I: A climatology. *Mon. Wea. Rev.*, **118**, 1103–1122, https://doi.org/10.1175/1520-0493(1990)118<1103:TAFSIE>2.0.CO;2.

Copernicus Climate Change Service, 2017: ERA5: Fifth generation of ECMWF atmospheric reanalyses of the global climate. Accessed 25 August 2023, https://cds.climate.copernicus.eu/cdsapp#!/home.

Corfidi, S. F., S. J. Corfidi, and D. M. Schultz, 2008: Elevated convection and castellanus: Ambiguities, significance, and questions. *Wea. Forecasting*, **23**, 1280–1303, https://doi.org/10.1175/2008WAF2222118.1.

Dennis, E. J., and M. R. Kumjian, 2017: The impact of vertical wind shear on hail growth in simulated supercells. *J. Atmos. Sci.*, **74**, 641–663, https://doi.org/10.1175/JAS-D-16-0066.1.

Dobur, J. C., 2005: A comparison of severe thunderstorm warning verification statistics and population density within the NWS Atlanta county warning area. Preprints, *Fourth Annual Severe Storms Symp.*, Starkville, MS, East Mississippi Chapter National Weather Association/Amer. Meteor. Soc., D2–6, https://www.weather.gov/media/ffc/SEconf.pdf.

Doswell, C. A., III, H. E. Brooks, and M. P. Kay, 2005: Climatological estimates of daily local nontornadic severe thunderstorm probability for the United States. *Wea. Forecasting*, **20**, 577–595, https://doi.org/10.1175/WAF866.1.

Elmore, K. L., Z. L. Flamig, V. Lakshmanan, B. T. Kaney, V. Farmer, H. D. Reeves, and L. P. Rothfusz, 2014: MPING: Crowd-sourcing weather reports for research. *Bull. Amer. Meteor. Soc.*, **95**, 1335–1342, https://doi.org/10.1175/BAMS-D-13-00014.1.

——, J. T. Allen, and A. E. Gerard, 2022: Sub-severe and severe hail. *Wea. Forecasting*, **37**, 1357–1369, https://doi.org/10.1175/WAF-D-21-0156.1.

Gensini, V. A., T. L. Mote, and H. E. Brooks, 2014: Severe-thunderstorm reanalysis environments and collocated radiosonde observations. *J. Appl. Meteor. Climatol.*, **53**, 742–751, https://doi.org/10.1175/JAMC-D-13-0263.1.

——, C. Converse, W. S. Ashley, and M. Taszarek, 2021: Machine learning classification of significant tornadoes and hail in the

United States using ERA5 proximity soundings. *Wea. Forecasting*, **36**, 2143–2160, https://doi.org/10.1175/WAF-D-21-0056.1.

Groenemeijer, P. H., and A. Van Delden, 2007: Sounding-derived parameters associated with large hail and tornadoes in the Netherlands. *Atmos. Res.*, **83**, 473–487, https://doi.org/10.1016/j.atmosres.2005.08.006.

——, and Coauthors, 2017: Severe convective storms in Europe: Ten years of research and education at the European Severe Storms Laboratory. *Bull. Amer. Meteor. Soc.*, **98**, 2641–2651, https://doi.org/10.1175/BAMS-D-16-0067.1.

Gunturi, P., and M. Tippett, 2017: Impact of ENSO on U.S. tornado and hail frequencies. Managing Severe Thunderstorm Risk Tech. Rep., 5 pp., http://www.columbia.edu/~mkt14/files/WillisRe_Impact_of_ENSO_on_US_Tornado_and_Hail_frequencies_Final.pdf.

Gutierrez, R. E., and M. R. Kumjian, 2021: Environmental and radar characteristics of gargantuan hail-producing storms. *Mon. Wea. Rev.*, **149**, 2523–2538, https://doi.org/10.1175/MWR-D-20-0298.1.

Hales, J. E., Jr., 1988: Improving the watch/warning program through use of significant event data. Preprints, *15th Conf. on Severe Local Storms*, Baltimore, MD, Amer. Meteor. Soc., 165–168.

Hersbach, H., and Coauthors, 2020: The ERA5 global reanalysis. *Quart. J. Roy. Meteor. Soc.*, **146**, 1999–2049, https://doi.org/10.1002/qj.3803.

Holton, J. R., 1973: A one-dimensional cumulus model including pressure perturbations. *Mon. Wea. Rev.*, **101**, 201–205, https://doi.org/10.1175/1520-0493(1973)101<0201:AOCMIP>2.3.CO;2.

Homeyer, C. R., and M. R. Kumjian, 2015: Microphysical characteristics of overshooting convection from polarimetric radar observations. *J. Atmos. Sci.*, **72**, 870–891, https://doi.org/10.1175/JAS-D-13-0388.1.

——, E. M. Murillo, and M. R. Kumjian, 2023: Relationships between 10 years of radar-observed supercell characteristics and hail potential. *Mon. Wea. Rev.*, **151**, 2609–2632, https://doi.org/10.1175/MWR-D-23-0019.1.

Horgan, K. L., D. M. Schultz, J. E. Hales Jr., S. F. Corfidi, and R. H. Johns, 2007: A five-year climatology of elevated severe convective storms in the United States east of the Rocky Mountains. *Wea. Forecasting*, **22**, 1031–1044, https://doi.org/10.1175/WAF1032.1.

Houston, A. L., R. L. Thompson, and R. Edwards, 2008: The optimal bulk wind differential depth and the utility of the upper-tropospheric storm-relative flow for forecasting supercells. *Wea. Forecasting*, **23**, 825–837, https://doi.org/10.1175/2008WAF2007007.1.

Jewell, R., and J. Brimelow, 2009: Evaluation of Alberta hail growth model using severe hail proximity soundings from the United States. *Wea. Forecasting*, **24**, 1592–1609, https://doi.org/10.1175/2009WAF2222230.1.

Johns, R. H., J. M. Davies, and P. W. Leftwich, 1993: Some wind and instability parameters associated with strong and violent tornadoes. 2. Variations in the combinations of wind and instability parameters. *The Tornado: Its Structure, Dynamics, Prediction, and Hazards*, *Geophys. Monogr.*, Vol. 79, Amer. Geophys. Union, 583–590, https://doi.org/10.1029/GM079p0583.

Johnson, A. W., and K. E. Sugden, 2014: Evaluation of sounding-derived thermodynamic and wind-related parameters associated with large hail events. *Electron. J. Severe Storms Meteor.*, **9** (5), https://doi.org/10.55599/ejssm.v9i5.57.

King, A. T., and A. D. Kennedy, 2019: North American supercell environments in atmospheric reanalyses and RUC-2. *J. Appl. Meteor. Climatol.*, **58**, 71–92, https://doi.org/10.1175/JAMC-D-18-0015.1.

Knight, C. A., and N. C. Knight, 2001: Hailstorms. *Severe Convective Storms*, *Meteor. Monogr.*, No. 50, Amer. Meteor. Soc., 223–254, https://doi.org/10.1175/0065-9401-28.50.223.

——, and ——, 2005: Very large hailstones from Aurora, Nebraska. *Bull. Amer. Meteor. Soc.*, **86**, 1773–1782, https://doi.org/10.1175/BAMS-86-12-1773.

Kohonen, T., 2013: Essentials of the self-organizing map. *Neural Networks*, **37**, 52–65, https://doi.org/10.1016/j.neunet.2012.09.018.

Kumjian, M. R., and K. Lombardo, 2020: A hail growth trajectory model for exploring the environmental controls on hail size: Model physics and idealized tests. *J. Atmos. Sci.*, **77**, 2765–2791, https://doi.org/10.1175/JAS-D-20-0016.1.

——, Z. J. Lebo, and A. M. Ward, 2019: Storms producing large accumulations of small hail. *J. Appl. Meteor. Climatol.*, **58**, 341–364, https://doi.org/10.1175/JAMC-D-18-0073.1.

——, K. Lombardo, and S. Loeffler, 2021: The evolution of hail production in simulated supercell storms. *J. Atmos. Sci.*, **78**, 3417–3440, https://doi.org/10.1175/JAS-D-21-0034.1.

Kuo, H. L., and W. H. Raymond, 1980: A quasi-one-dimensional cumulus cloud model and parameterization of cumulus heating and mixing effects. *Mon. Wea. Rev.*, **108**, 991–1009, https://doi.org/10.1175/1520-0493(1980)108<0991:AQODCC>2.0.CO;2.

Lasher-Trapp, S., E. Jo, L. R. Allen, B. N. Engelsen, and R. J. Trapp, 2021: Entrainment in a simulated supercell thunderstorm. Part I: The evolution of different entrainment mechanisms and their dilutive effects. *J. Atmos. Sci.*, **78**, 2725–2740, https://doi.org/10.1175/JAS-D-20-0223.1.

Lin, Y., and M. R. Kumjian, 2022: Influences of CAPE on hail production in simulated supercell storms. *J. Atmos. Sci.*, **79**, 179–204, https://doi.org/10.1175/JAS-D-21-0054.1.

Mann, H. B., and D. R. Whitney, 1947: On a test of whether one of two random variables is stochastically larger than the other. *Ann. Math. Stat.*, **18**, 50–60, https://doi.org/10.1214/aoms/1177730491.

Mead, C. M., and R. L. Thompson, 2011: Environmental characteristics associated with nocturnal significant-tornado events in the Great Plains. *Electron. J. Severe Storms Meteor.*, **6** (6), https://doi.org/10.55599/ejssm.v6i6.33.

Miller, L. J., J. D. Tuttle, and C. A. Knight, 1988: Airflow and hail growth in a severe northern High Plains supercell. *J. Atmos. Sci.*, **45**, 736–762, https://doi.org/10.1175/1520-0469(1988)045<0736:AAHGIA>2.0.CO;2.

Mulholland, J. P., J. M. Peters, and H. Morrison, 2021: How does LCL height influence deep convective updraft width? *Geophys. Res. Lett.*, **48**, e2021GL093316, https://doi.org/10.1029/2021GL093316.

Murillo, E. M., and C. R. Homeyer, 2019: Severe hail fall and hailstorm detection using remote sensing observations. *J. Appl. Meteor. Climatol.*, **58**, 947–970, https://doi.org/10.1175/JAMC-D-18-0247.1.

——, ——, and J. T. Allen, 2021: A 23-year severe hail climatology using GridRad MESH observations. *Mon. Wea. Rev.*, **149**, 945–958, https://doi.org/10.1175/MWR-D-20-0178.1.

Nelson, S. P., 1983: The influence of storm flow structure on hail growth. *J. Atmos. Sci.*, **40**, 1965–1983, https://doi.org/10.1175/1520-0469(1983)040<1965:TIOSFS>2.0.CO;2.

Nixon, C. J., and J. T. Allen, 2022: Distinguishing between hodographs of severe hail and tornadoes. *Wea. Forecasting*, **37**, 1761–1782, https://doi.org/10.1175/WAF-D-21-0136.1.

Nowotarski, C. J., and A. A. Jensen, 2013: Classifying proximity soundings with self-organizing maps toward improving supercell and tornado forecasting. *Wea. Forecasting*, **28**, 783–801, https://doi.org/10.1175/WAF-D-12-00125.1.

——, and E. A. Jones, 2018: Multivariate self-organizing map approach to classifying supercell tornado environments using near-storm, low-level wind and thermodynamic profiles. *Wea. Forecasting*, **33**, 661–670, https://doi.org/10.1175/WAF-D-17-0189.1.

Peters, J. M., C. J. Nowotarski, and H. Morrison, 2019: The role of vertical wind shear in modulating maximum supercell updraft velocities. *J. Atmos. Sci.*, **76**, 3169–3189, https://doi.org/10.1175/JAS-D-19-0096.1.

——, H. Morrison, C. J. Nowotarski, J. P. Mulholland, and R. L. Thompson, 2020a: A formula for the maximum vertical velocity in supercell updrafts. *J. Atmos. Sci.*, **77**, 3747–3757, https://doi.org/10.1175/JAS-D-20-0103.1.

——, C. J. Nowotarski, J. P. Mulholland, and R. L. Thompson, 2020b: The influences of effective inflow layer streamwise vorticity and storm-relative flow on supercell updraft properties. *J. Atmos. Sci.*, **77**, 3033–3057, https://doi.org/10.1175/JAS-D-19-0355.1.

——, D. R. Chavas, C.-Y. Su, H. Morrison, and B. E. Coffer, 2023: An analytic formula for entraining CAPE in midlatitude storm environments. *J. Atmos. Sci.*, **80**, 2165–2186, https://doi.org/10.1175/JAS-D-23-0003.1.

Pilguj, N., M. Taszarek, J. T. Allen, and K. A. Hoogewind, 2022: Are trends in convective parameters over the United States and Europe consistent between reanalyses and observations? *J. Climate*, **35**, 3605–3626, https://doi.org/10.1175/JCLI-D-21-0135.1.

Pilorz, W., M. Zięba, J. Szturc, and E. Łupikasza, 2022: Large hail detection using radar-based VIL calibrated with isotherms from the ERA5 reanalysis. *Atmos. Res.*, **274**, 106185, https://doi.org/10.1016/j.atmosres.2022.106185.

Potvin, C. K., K. L. Elmore, and S. J. Weiss, 2010: Assessing the impacts of proximity sounding criteria on the climatology of significant tornado environments. *Wea. Forecasting*, **25**, 921–930, https://doi.org/10.1175/2010WAF2222368.1.

Púčik, T., P. Groenemeijer, D. Rýva, and M. Kolář, 2015: Proximity soundings of severe and nonsevere thunderstorms in central Europe. *Mon. Wea. Rev.*, **143**, 4805–4821, https://doi.org/10.1175/MWR-D-15-0104.1.

——, C. Castellano, P. Groenemeijer, T. Kühne, A. T. Rädler, B. Antonescu, and E. Faust, 2019: Large hail incidence and its economic and societal impacts across Europe. *Mon. Wea. Rev.*, **147**, 3901–3916, https://doi.org/10.1175/MWR-D-19-0204.1.

Rasmussen, R. M., and A. J. Heymsfield, 1987: Melting and shedding of graupel and hail. Part I: Model physics. *J. Atmos. Sci.*, **44**, 2754–2763, https://doi.org/10.1175/1520-0469(1987)044<2754:MASOGA>2.0.CO;2.

Reges, H. W., N. Doesken, J. Turner, N. Newman, A. Bergantino, and Z. Schwalbe, 2016: CoCoRaHS: The evolution and accomplishments of a volunteer rain gauge network. *Bull. Amer. Meteor. Soc.*, **97**, 1831–1846, https://doi.org/10.1175/BAMS-D-14-00213.1.

Schaefer, J. T., and J. Galway, 1982: Population biases in tornado climatology. Preprints, *12th Conf. on Severe Local Storms*, San Antonio, TX, Amer. Meteor. Soc., 51–54.

——, and R. Edwards, 1999: The SPC tornado/severe thunderstorm database. Preprints, *11th Conf. on Applied Climatology*, Dallas, TX, Amer. Meteor. Soc., 215–220.

——, J. J. Levit, S. J. Weiss, and D. W. McCarthy, 2004: The frequency of large hail over the contiguous United States. Preprints, *14th Conf. on Applied Climatology*, Seattle, WA, Amer. Meteor. Soc., 3.3, http://ams.confex.com/ams/pdfpapers/69834.pdf.

Sherburn, K. D., and M. D. Parker, 2014: Climatology and ingredients of significant severe convection in high-shear, low-CAPE environments. *Wea. Forecasting*, **29**, 854–877, https://doi.org/10.1175/WAF-D-13-00041.1.

Smith, B. T., R. L. Thompson, J. S. Grams, C. Broyles, and H. E. Brooks, 2012: Convective modes for significant severe thunderstorms in the contiguous United States. Part I: Storm classification and climatology. *Wea. Forecasting*, **27**, 1114–1135, https://doi.org/10.1175/WAF-D-11-00115.1.

Storer, R. L., and S. C. van den Heever, 2013: Microphysical processes evident in aerosol forcing of tropical deep convective clouds. *J. Atmos. Sci.*, **70**, 430–446, https://doi.org/10.1175/JAS-D-12-076.1.

Storm Prediction Center, 2019: Significant hail parameter. Accessed 25 August 2023, https://www.spc.noaa.gov/exper/mesoanalysis/help/help_sigh.html.

Taszarek, M., H. E. Brooks, and B. Czernecki, 2017: Sounding-derived parameters associated with convective hazards in Europe. *Mon. Wea. Rev.*, **145**, 1511–1528, https://doi.org/10.1175/MWR-D-16-0384.1.

——, ——, ——, P. Szuster, and K. Fortuniak, 2018: Climatological aspects of convective parameters over Europe: A comparison of ERA-Interim and sounding data. *J. Climate*, **31**, 4281–4308, https://doi.org/10.1175/JCLI-D-17-0596.1.

——, J. T. Allen, T. Púčik, K. A. Hoogewind, and H. E. Brooks, 2020: Severe convective storms across Europe and the United States. Part II: ERA5 environments associated with lightning, large hail, severe wind, and tornadoes. *J. Climate*, **33**, 10 263–10 286, https://doi.org/10.1175/JCLI-D-20-0346.1.

——, ——, H. E. Brooks, N. Pilguj, and B. Czernecki, 2021a: Differing trends in United States and European severe thunderstorm environments in a warming climate. *Bull. Amer. Meteor. Soc.*, **102**, E296–E322, https://doi.org/10.1175/BAMS-D-20-0004.1.

——, N. Pilguj, J. T. Allen, V. Gensini, H. E. Brooks, and P. Szuster, 2021b: Comparison of convective parameters derived from ERA5 and MERRA-2 with rawinsonde data over Europe and North America. *J. Climate*, **34**, 3211–3237, https://doi.org/10.1175/JCLI-D-20-0484.1.

Thompson, R. L., C. M. Mead, and R. Edwards, 2007: Effective storm-relative helicity and bulk shear in supercell thunderstorm environments. *Wea. Forecasting*, **22**, 102–115, https://doi.org/10.1175/WAF969.1.

——, B. T. Smith, J. S. Grams, A. R. Dean, and C. Broyles, 2012: Convective modes for significant severe thunderstorms in the contiguous United States. Part II: Supercell and QLCS tornado environments. *Wea. Forecasting*, **27**, 1136–1154, https://doi.org/10.1175/WAF-D-11-00116.1.

Warren, R. A., H. Richter, H. A. Ramsay, S. T. Siems, and M. J. Manton, 2017: Impact of variations in upper-level shear on simulated supercells. *Mon. Wea. Rev.*, **145**, 2659–2681, https://doi.org/10.1175/MWR-D-16-0412.1.

——, ——, and R. L. Thompson, 2021: Spectrum of near-storm environments for significant severe right-moving supercells in the contiguous United States. *Mon. Wea. Rev.*, **149**, 3299–3323, https://doi.org/10.1175/MWR-D-21-0006.1.

Zhou, Z., Q. Zhang, J. T. Allen, X. Ni, and C.-P. Ng, 2021: How many types of severe hailstorm environments are there globally? *Geophys. Res. Lett.*, **48**, e2021GL095485, https://doi.org/10.1029/2021GL095485.